AD-A169 531 PNS (PARABOLIZED NAVIER-STOKES) FOR SPINNING SHELL AT 1/1
MODERATE ANGLES OF..(U) ARMY BALLISTIC RESEARCH LAB
ABERDEEN PROVING GROUND MD P WEINACHT ET AL. JUN 86
UNCLASSIFIED BRL-MR-3522 F/G 20/4 NL

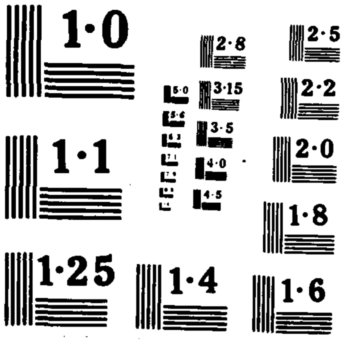
1·0
2·8
2·5
5·0
3·15
2·2
5·6
3·5
1·1
4·0
2·0
4·5
1·8
1·25
1·4
1·6

(12)

MEMORANDUM REPORT BRL-MR-3522

PNS COMPUTATIONS FOR SPINNING SHELL AT MODERATE ANGLES OF ATTACK AND FOR LONG L/D FINNED PROJECTILES

Paul Weinacht
Bernard J. Guidos
Walter B. Sturek
Betty Ann Hodes

June 1986

US ARMY BALLISTIC RESEARCH LABORATORY
ABERDEEN PROVING GROUND, MARYLAND

UNCLASSIFIED

SECURITY CLASSIFICATION OF THIS PAGE (When Data Entered)

REPORT DOCUMENTATION PAGE	READ INSTRUCTIONS BEFORE COMPLETING FORM
1. REPORT NUMBER Memorandum Report BRL-MR-3522	2. GOVT ACCESSION NO. AD-A169531 3. RECIPIENT'S CATALOG NUMBER
4. TITLE (and Subtitle) PNS COMPUTATIONS FOR SPINNING SHELL AT MODERATE ANGLES OF ATTACK AND FOR LONG L/D FINNED PROJECTILES	5. TYPE OF REPORT & PERIOD COVERED FINAL 6. PERFORMING ORG. REPORT NUMBER
7. AUTHOR(s) Paul Weinacht, Bernard J. Guidos, Walter B. Sturek and Betty Ann Hodes	8. CONTRACT OR GRANT NUMBER(s)
9. PERFORMING ORGANIZATION NAME AND ADDRESS U.S. Army Ballistic Research Laboratory ATTN: SLCBR-LF Aberdeen Proving Ground, Maryland 21005-5066	10. PROGRAM ELEMENT, PROJECT, TASK AREA & WORK UNIT NUMBERS RDT&E 1L162618AH80
11. CONTROLLING OFFICE NAME AND ADDRESS U.S. Army Ballistic Research Laboratory ATTN: SLCBR-DD-T Aberdeen Proving Ground, Maryland 21005-5066	12. REPORT DATE June 1986 13. NUMBER OF PAGES 46
14. MONITORING AGENCY NAME & ADDRESS(if different from Controlling Office)	15. SECURITY CLASS. (of this report) UNCLASSIFIED 15a. DECLASSIFICATION/DOWNGRADING SCHEDULE

16. DISTRIBUTION STATEMENT (of this Report)

Approved for public release, distribution unlimited.

17. DISTRIBUTION STATEMENT (of the abstract entered in Block 20, if different from Report)

18. SUPPLEMENTARY NOTES

19. KEY WORDS (Continue on reverse side if necessary and identify by block number)

Computational Fluid Dynamics	Parabolized Navier-Stokes
Finned Projectiles	Spinning Projectiles
Supersonic Viscous Flow	Turbulence Modeling
Long L/D Projectiles	High Angle of Attack Aerodynamics

20. ABSTRACT (Continue on reverse side if necessary and identify by block number)

The thin-layer Parabolized Navier-Stokes (PNS) computational technique is applied to calculate the three-dimensional viscous flow about two types of projectiles: (1) a standard shell configuration at moderate angle of attack with a region of lee side crossflow separation and (2) long L/D finned projectiles. Results for the shell configuration are obtained using the algebraic turbulence model for Baldwin and Lomax with and without modifications that more properly account for regions of lee side crossflow separation. Comparisons are

DD FORM 1 JAN 73 1473 EDITION OF 1 NOV 65 IS OBSOLETE

UNCLASSIFIED

SECURITY CLASSIFICATION OF THIS PAGE (When Data Entered)

20. ABSTRACT (Continued)

made with wind tunnel pressure and force measurments as well as boundary layer velocity data. For a nonspinning shell, significant improvement in prediction of surface pressure at 6.3 degrees angle of attack is found by applying the modified model. For spinning shell, good agreement between the numerical predictions and the experimental Magnus force and velocity profile data is found only if the turbulence model modification strategy is relaxed. Results are then presented for the long L/D finned projectile configurations. Computed pitch-plane aerodynamic coefficients for long L/D axisymmetric forebodies (20-35 calibers) are presented and compared with wind tunnel data. The results, which are in reasonable agreement with the experimental data, demonstrate the importance of viscous effects on the pitch plane aerodynamics for long L/D bodies. Computations for a complete finned body configuration are presented and comparison made with inviscid code predictions and aerodynamic range data. Good agreement between the PNS computations, the inviscid predictions, and the range data is observed.

TABLE OF CONTENTS

Page

LIST OF ILLUSTRATIONS 5

I. INTRODUCTION 9

II. COMPUTATIONAL TECHNIQUE 10
   A. Space Marching Procedure 11
   B. Conical Starting Solutions 12
   C. Turbulence Model 12
      1. Baldwin and Lomax Model 12
      2. Turbulence Model Modification 14

III. RESULTS 15
   A. Shell Configuration at Moderate Angle of Attack 15
      1. Nonspin Case 16
      2. Spin Case 17
   B. Long L/D Finned Body Configurations 17
      1. Forebodies 17
      2. Finned Projectile Configuration 19

IV. CONCLUSIONS 22
   A. Computations at Moderate Angle of Attack 22
   B. Computations for Long L/D Finned Body Configuration 22

ACKNOWLEDGMENT 22

REFERENCES 41

LIST OF SYMBOLS 43

DISTRIBUTION LIST 45

LIST OF ILLUSTRATIONS

Figure Page

1 Grid Coordinates and Notation 23

2 Circumferential Variation of F_{max} for SOC and SOCBT Configurations; $M = 3$, $\alpha = 6.3^\circ$, $PD/V = 0$, $Re = 2.13 \times 10^7/m$, $X/D = 4.29$ 23

3 Circumferential Variation of y_{max} for SOC and SOCBT Configurations; $M = 3$, $\alpha = 6.3^\circ$, $PD/V = 0$, $Re = 2.13 \times 10^7/m$, $X/D = 4.29$ 24

4 Secant Ogive-Cylinder-Boattail (SOCBT) Model Configuration 24

5a Region of Crossflow Separation for SOC Configuration $M = 3$, $\alpha = 6.3^\circ$, $PD/V = 0$, $Re = 2.13 \times 10^7/m$ 25

5b Region of Crossflow Separation for SOCBT Configuration $M = 3$, $\alpha = 6.3^\circ$, $PD/V = 0$, $Re = 2.13 \times 10^7/m$ 25

6 Longitudinal Surface Pressure Distribution for SOCBT Configuration; $M = 3$, $\alpha = 6.3^\circ$, $PD/V = 0$, $Re = 2.13 \times 10^7/m$ 26

7 Circumferential Surface Pressure Distribution for SOCBT Configuration; $M = 3$, $\alpha = 6.3^\circ$, $PD/V = 0$, $Re = 2.13 \times 10^7/m$, $X/D = 5.77$ 26

8 Longitudinal Velocity Profiles for SOCBT Configuration; $M = 3$, $\alpha = 6.3^\circ$, $PD/V = 0$, $Re = 2.13 \times 10^7/m$, $X/D = 5.67$ 27

9a Longitudinal Velocity Profile for SOCBT Configuration, $M = 3$, $\alpha = 6.3^\circ$, $PD/V = 0$, $Re = 2.13 \times 10^7/m$, $X/D = 5.67$, $\phi = 120^\circ$ 27

9b Longitudinal Velocity Profile for SOCBT Configuration; $M = 3$, $\alpha = 6.3^\circ$, $PD/V = 0$, $Re = 2.13 \times 10^7/m$, $X/D = 5.67$, $\phi = 150^\circ$ 28

9c Longitudinal Velocity Profile for SOCBT Configuration; $M = 3$, $\alpha = 6.3^\circ$, $PD/V = 0$, $Re = 2.13 \times 10^7/m$, $X/D = 5.67$, $\phi = 180^\circ$ 28

10 Sign Convention for Spin and Aerodynamic Force Coefficients 29

11 Total Magnus Force Coefficient Developing over SOCBT Configuration; $M = 3$, $\alpha = 6.3^\circ$, $PD/V = .19$, $Re = 2.13 \times 10^7/m$ 29

12a Longitudinal Velocity Profile for SOCBT Configuration; $M = 3$, $\alpha = 6.3^\circ$, $PD/V = .19$, $Re = 2.13 \times 10^7/m$, $X/D = 5.67$, $\phi = 120^\circ$ 30

LIST OF ILLUSTRATIONS (Continued)

Figure		Page
12b	Longitudinal Velocity Profile for SOCBT Configuration; $M = 3$, $\alpha = 6.3°$, $PD/V = .19$, $Re = 2.13 \times 10^7/m$, $X/D = 5.67$, ϕ 210°	30
12c	Longitudinal Velocity Profile for SOCBT Configuration; $M = 3$, $\alpha = 6.3°$, $PD/V = .19$, $Re = 2.13 \times 10^7/m$, $X/D = 5.67$, $\phi = 240°$	31
13	Forebody Configuration	31
14	Development of Normal Force Coefficient along Body for Varying Circumferential Resolution, $M = 4$, $\alpha = 2°$, $Re_D = 3.2 \times 10^6$	32
15	Development of Normal Force Coefficient along Body, $M = 4$, $\alpha = 2°$, $Re_D = 0.41 \times 10^6$	32
16	Development of Pitching Moment Coefficient along Body, $M = 4$, $\alpha = 2°$, $Re_D = 0.41 \times 10^6$	33
17	Development of Normal Force Coefficient along Body, $M = 5$, $\alpha = 2°$, $Re_D = 0.54 \times 10^6$	33
18	Development of Pitching Moment Coefficient along Body, $M = 5$, $\alpha = 2°$, $Re_D = 0.54 \times 10^6$	34
19	Development of Normal Force Coefficient over Long L/D Axisymmetric Body, Effect of Mach and Reynold's Numbers, $\alpha = 2°$	34
20	Finned Projectile Configuration	35
21	Shadowgraph of M735 in Flight	35
22	Grid on Body Surface on Finned Portion of Projectile	36
23a	Cross Section of Grid at $X/D = 13.2$, Half Plane Grid	37
23b	Cross Section of Grid at $X/D = 13.2$, Close-Up of Grid Near Body	37
24	Axial Pressure Distribution at $\phi = 0°$, 90° and 180°, $M = 4$, $\alpha = 2°$, $Re_D = 3.2 \times 10^6$	38
25	Development of Normal Force Coefficient along the Body, $M = 4$, $\alpha = 2°$, $Re_D, = 3.2 \times 10^6$	38
26	Zero-Degree Slope of the Normal Force Coefficient versus Mach Number	39

LIST OF ILLUSTRATIONS (Continued)

Figure Page

27 Zero-Degree Slope of the Pitching Moment Coefficient versus Mach Number........ 39

INTRODUCTION

Application of the Parabolized Navier-Stokes (PNS) technique to predict the three-dimensional viscous flow about slender bodies of revolution at supersonic speeds and small angles of attack has been performed in the past with a considerable degree of success.[1] Of particular significance to the U.S. Army is the capability that this technique provides in the prediction of the Magnus force and moment for spinning shell at small angles of attack.[2, 3] Current efforts in the prediction of the aerodynamics of U.S. Army projectiles in supersonic flight are directed towards extending the applicability of the PNS technique for the calculation of more complicated flows. Two such applications are discussed in this report; the first involves solution of the flow about a spinning axisymmetric projectile at six degrees angle of attack with a region of lee side crossflow separation, and, the second, the calculation of the flow around long L/D finned bodies.

Previous studies[1, 2, 4] have presented accurate predictions of pitch plane aerodynamic coefficients for axisymmetric projectiles to angles of attack greater than ten degrees. However, accurate predictions of Magnus (side) force and moment have been limited to angles of attack between zero and six degrees. This is due, in part, to the inability of the Baldwin-Lomax turbulence model[5] to properly model regions of lee side crossflow separation. Degani and Schiff,[6] who applied the PNS technique to examine the high angle of

---

1. *W.B. Sturek, D.C. Mylin and C.C. Bush, "Computational Parametric Study of the Aerodynamics of Spinning Bodies at Supersonic Speeds," U.S. Army Ballistic Research Laboratory, Aberdeen Proving Ground, Maryland, ARBRL-TR-02358, August 1981. (AD A106074)*

2. *W.B. Sturek and L.B. Schiff, "Computations of the Magnus Effect for Slender Bodies in Supersonic Flow," U.S. Army Ballistic Research Laboratory, Aberdeen Proving Ground, Maryland, ARBRL-TR-02384, December 1981. (AD A110016)*

3. *L.B. Schiff and W.B. Sturek, "Numerical Simulation of Steady Supersonic Flow Over an Ogive Cylinder Boattail Body," U.S. Army Ballistic Research Laboratory, Aberdeen Proving Ground, Maryland, ARBRL-TR-02363, September 1981. (AD A106060)*

4. *M. McWerter, R.W. Noack and W.L. Oberkampf, "Evaluation of Inviscid/Boundary Layer and Parabolized Navier-Stokes Solutions for Design of Reentry Vehicles," AIAA Paper No. 84-0486, 22nd Aerospace Sciences Meeting, January 1984.*

5. *B.S. Baldwin and H. Lomax, "Thin Layer Approximation and Algebraic Model for Separated Turbulent Flows," AIAA Paper No. 78-257, 16th Aerospace Sciences Meeting, January 1978.*

6. *D. Degani and L.B. Schiff, "Computation of Supersonic Viscous Flows Around Pointed Bodies at Large Incidence," AIAA Paper No. 83-0034, 21st Aerospace Sciences Meeting, January 1983.*

attack flow about cones and a Secant-Ogive-Cylinder (SOC) projectile configuration, concluded that near regions of crossflow separation the values of the eddy viscosity obtained from the Baldwin and Lomax model were much too high. To overcome this problem, they applied, with a significant degree of success, an approach which limits the eddy viscosity to values that are more realistic. In this report, modifications similar to those of Degani and Schiff are applied to computations for a Secant-Ogive-Cylinder-Boattail (SOCBT) projectile configuration at 6.3 degrees angle of attack, Mach 3, with and without spin. The results are compared to predictions obtained with the original Baldwin and Lomax turbulence model and to wind tunnel measurements.

The second set of results presented in this report concerns the application of the PNS technique to predict the aerodynamics of long L/D finned bodies. Quite recently, several papers have reported the application of the PNS technique to examine the aerodynamic of finned body configurations.[7-10] The computations for the finned body configuration examined in Reference 10, resembling a long L/D kinetic energy (KE) penetrator projectile, were, in the opinion of the authors, not fully successful. Solutions over the finned portion of the body were only obtained using large amounts of smoothing and a coarse grid near the fin surface. Additionally, it was later discovered that increased circumferential grid resolution is required over the long L/D axisymmetric forebody. The results presented in this report address these areas of deficiency in the previous calculation. Predicted pitch-plane aerodynamic coefficients for long L/D (20-35 caliber) axisymmetric kinetic energy penetrator forebodies at Mach 4 and 5, and two degrees angle of attack, are presented and compared with available wind tunnel data. Significantly improved results are then presented for a complete finned body configuration at Mach numbers 3, 4 and 5, and two degrees angle of attack.

II. COMPUTATIONAL TECHNIQUE

Calculation of the flow field over the body is accomplished using the Parabolized Navier-Stokes technique. The PNS technique allows the solution to

---

[7] *M.M. Rai and D.S. Chaussee, "New Implicit Boundary Procedures: Theory and Applications," AIAA Paper No. 83-0123, 21st Aerospace Sciences Meeting, January 1983.*

[8] *M.M. Rai, D.S. Chaussee and Y.M. Risk, "Calculation of Viscous Supersonic Flows Over Finned Bodies," AIAA Paper No. 83-1667, Danvers, MA, July 1983.*

[9] *J.W. Jettmar, "Calculations of Viscous Supersonic Flow Over Finned Bodies Using a 'Thin-Fin' Approximation," AIAA Paper No. 84-2114, AIAA Atmospheric Flight Mechanics Conference, August 1984.*

[10] *P. Weinacht, F.J. Guidos, L.D. Kayser and W.B. Sturek, "PNS Computations for Spinning and Fin-Stabilized Projectiles at Supersonic Velocities," AIAA Paper No. 84-2118, AIAA Atmospheric Flight Mechanics Conference, August 1984. (BRL Memorandum Report to be published)*

be spacially marched along the body in the main flow direction due to the parabolic nature of the governing equations. An initial plane of data is required to begin the space marching procedure and may be obtained either from an auxiliary calculation or from a conical starting procedure, as has been done for the results presented here. Both the space marching and conical starting procedures are outlined below.

A. Space Marching Procedure

The thin-layer Parabolized Navier-Stokes computational technique developed by Schiff and Steger[11] has been employed to calculate the flow downstream of the nose tip. The governing steady thin-layer equations in strong conservative form and generalized coordinates are written below:

$$\frac{\partial \hat{E}_s}{\partial \xi} + \frac{\partial \hat{F}}{\partial \eta} + \frac{\partial \hat{G}}{\partial \zeta} = \frac{1}{\hat{Re}} \frac{\partial \hat{S}}{\partial \zeta} \qquad (1)$$

where ξ, η, ζ are the generalized coordinate variables as displayed in Figure 1 and defined below.

$\xi = \xi(x)$ is the longitudinal (marching) coordinate

$\eta = \eta(x,y,z)$ is the circumferential coordinate

$\zeta = \zeta(x,y,z)$ is the near normal coordinate.

This vector equation represents the thin-layer approximation to the equations of mass, momentum and energy conservation in the three coordinate directions. The inviscid flux vectors $\hat{E}_s$, $\hat{F}$ and $\hat{G}$ and the matrix of viscous terms, $\hat{S}$, are functions of the dependent variables represented by the vector, $q(\rho, \rho u, \rho v, \rho w, e)$, where ρ is the density; u, v and w are the velocity components in the three spacial directions x, y and z; and e is the total energy per unit volume.

The parabolized Navier-Stokes equations are solved using a conservative, approximately factored, implicit, finite-difference numerical algorithm as formulated by Beam and Warming.[12] Further details of the numerical method may be found in Reference 11. Fitting of the outer bow shock has been performed

---

[11] *L.B. Schiff and J.L. Steger, "Numerical Simulation of Steady Supersonic Viscous Flow," AIAA Paper No. 79-0130, 17th Aerospace Sciences Meeting, January 1979.*

[12] *R. Beam and R.F. Warming, "An Implicit Factored Scheme for the Compressible Navier-Stokes Equations," AIAA Journal, Vol. 16, No. 4, 1978, pp. 85-129.*

in these calculations, and details of the implicit boundary procedure as implemented by Rai and Chaussee may be found in Reference 7.

B. Conical Starting Solutions

The initial plane of data required to begin the marching procedure is obtained using the marching code by assuming conical flow at the tip of the projectile. By selecting a conical grid and initially setting the flow field variables to the free stream values, the solution is marched one step down the body. The solution is then scaled back to the original station according to the conical flow assumption and again marched a single step. This procedure is repeated until a converged solution is obtained. The convergence criterion for the conical starting solutions applied here was that the change in density between successive iterations was less than 10^{-5} times the free stream value for each of the points on the body. This converged solution is then used as the initial plane of data in the marching procedure.

It should be noted that for calculations involving spinning projectiles, the conical starting procedure introduces a small error since the circumferential velocity at the body surface changes with longitudinal position, violating the conical flow assumption. This error is small, however, and the correct circumferential velocity at the body surface is accounted for as the solution is marched downstream.

C. Turbulence Model

A fully turbulent boundary layer has been simulated in each of the reported PNS calculations using a two-layer eddy viscosity model. For the long L/D forebody and the finned body configurations, the original turbulence model of Baldwin and Lomax[5] was applied. Moderate angle of attack solutions for the axisymmetric shell configuration were obtained using both the original Baldwin and Lomax model and the modified model. Both of these models are described below.

1. Baldwin and Lomax Model.

The two-layer, Cebeci-type, algebraic turbulence model reported by Baldwin and Lomax[5] been used with considerable success throughout many applications of the thin-layer Navier-Stokes codes. The model accounts for the effects of turbulence through an eddy viscosity coefficient, μ_t, and utilizes a purely local analysis of the turbulent region.

In the original formulation of the Baldwin-Lomax turbulence model, the turbulent eddy viscosity coefficient, μ_t, is defined separately in an inner region, close to the body, and an outer region, as shown below;

$$\mu_t = \begin{cases} (\mu_t)_{\text{inner}} & y \leq y_c \\ (\mu_t)_{\text{outer}} & y_c < y \end{cases} \tag{2}$$

where y is the radial distance from the body surface and y_c is the smallest value of y at which the inner and outer values of μ_t are equal.

Within the inner region, the turbulent eddy viscosity coefficient is defined using a mixing length model

$$(\mu_t)_{inner} = \rho\ \ell^2\ |\omega| \tag{3}$$

where the length scale, ℓ, is defined as

$$\ell = ky\ [1 - \exp(-y^+/A^+)]. \tag{4}$$

k and A^+ are constants, $|\omega|$ is the magnitude of the local vorticity vector, and y^+ is the nondimensional boundary layer coordinate defined below,

$$y^+ = \frac{\sqrt{\rho_w\ \tau_w}}{\mu_w}\ y. \tag{5}$$

The subscript "w" represents the values at the body surface.

In the outer region, for attached boundary layers, the turbulent eddy viscosity is defined

$$(\mu_t)_{outer} = K\ C_{cp}\rho F_{WAKE}\ F_{KLEB}(y) \tag{6}$$

where K and C_{cp} are constants, and $F_{FLEB}(y)$ is the Klebanoff intermittency factor, which is equal to 1 at the wall, and decreases out from the wall. F_{WAKE} is given by

$$F_{WAKE} = y_{max}\ F_{max} \tag{7}$$

where F_{max} and y_{max} are determined from the function

$$F(y) = y\ |\omega|\ [1. - \exp\ (-y^+/A^+)] \tag{8}$$

F_{max} is the maximum value of F(y) along a radial profile from the wall to the boundary layer edge. The value of y at which this maximum occurs is defined as y_{max}. Further details of the model can be found in Reference 5.

For analysis of the turbulent boundary layer along projectiles at small angles of attack ($0 < \alpha < 4$), the Baldwin-Lomax model performs satisfactorily due, in part, to the well-behaved variations of F_{max} and y_{max}, both axially and circumferentially. The lack of crossflow separation allows a local profile of F(y) to attain a single, well-defined peak. Accuracy in the selection of the exact location of a peak in F(y) is enhanced by fitting a curve between three radial grid points at every body location.

2. Turbulence Model Modification. In order to obtain successful predictions of flow fields containing regions of crossflow separation, modifications to the original Baldwin and Lomax model have been necessary. The approach reported by Degani and Schiff[6] has been adopted here in an initial attempt to compute the complex flow behavior associated with crossflow separation and to determine the extent to which such a strategy may be applied to spinning and nonspinning boattailed projectiles.

In Reference 6, computations for a nonspinning Secant-Ogive-Cylinder (no boattail) projectile configuration revealed that the values of the outer eddy viscosity calculated by the original Baldwin-Lomax model were much too high in the regions of crossflow separation. The cause was determined to be an ambiguity in determining the peak in F(y) (Equation 8). Over much of the leeward side of the projectile, the radial profile of F(y) developed a second, extraneous peak due to the shedding of a vortex sheet associated with crossflow separation at six degrees angle of attack and greater. The behavior of the function F(y) caused a meaningless length scale to be chosen. This same behavior of the function F(y) was also repeatedly observed during the course of the current study.

The strategy implemented here is similar to that of Degani and Schiff: limit the values of F_{max} and y_{max} obtained by the original model by anticipating the uncontrolled growth of the function F(y). For each axial station, a maximum value of the scaling length y_{max} is defined as 1.8 times the value of y_{max} on the windward ray.

The implementation proceeds for each roll angle, starting from the windward ray and ending along the leeward ray. When the local y_{max} exceeds the maximum allowed y_{max}, it is "clipped" to the maximum allowed value. F_{max} and y_{max} are then frozen with respect to roll angle until the local value of y_{max} is again found to lie within the maximum allowed value. A peak in F(y) is defined if the value of F(y) drops below 90% of the local maximum. Where two separate, distinct peaks in F(y) exist, the peak closer to the body is chosen. If the two peaks in F(y) merge into one abnormally large peak (or a peak cannot be found at all), the value of F_{max} is frozen at the value used for the previous roll angle and the value of y_{max} is set equal to 1.8 times the value on the windward side.

Figures 2 and 3 show the representative behavior of F_{max} and y_{max} for the original and modified Baldwin-Lomax formulations for the nonspinning SOCBT at six degrees angle of attack. At each longitudinal position, constant values of F_{max} and y_{max} are assigned over much of the leeward face of the projectile. The longitudinal variation, although not shown here, varies smoothly since it is controlled by the smooth behavior on the windward side. It is worth noting here that the cutoff points for F_{max} and y_{max} in Figure 2 do not necessarily represent the roll angles where crossflow separation actually occurs; they merely reflect the factor of 1.8 being introduced into the selection process. Furthermore, interpolating between three radial points to increase the accuracy of the peak locations of F(y) was discontinued whereever the cutoff strategy was applied.

III. RESULTS

A. Shell Configuration at Moderate Angle of Attack

Results were obtained primarily for the six caliber SOCBT configuration shown in Figure 4 at Mach 3, 6.3 degrees angle of attack, with and without spin, for flow conditions duplicating that of the experiments.[13-15] Additional results were also computed for the same projectile with no boattail (SOC) to establish effects of presence of a 7° boattail.

The grid for these computations consisted of 45 exponentially stretched points between the body and the shock and an equal spacing of points circumferentially at 5° increments. For the case of zero spin, calculations were performed in a half plane by applying a symmetry boundary condition along the midplane of the body, while the computations with spin were carried out in a full circumferential plane. To properly resolve the viscous effects, the radial grid resolution at the body surface was controlled such that the nondimensional boundary layer coordinate, y^+, was approximately 5 at the first point above the wall for all roll angles. This was accomplished through the

---

13. *R.P. Reklis and W.B. Sturek, "Surface Pressure Measurements on Slender Bodies at Angle of Attack at Supersonic Speeds," U.S. Army Ballistic Research Laboratory, Aberdeen Proving Ground, Maryland, ARBRL-MR-02876, November 1978. (AD A064097)*

14. *C.J. Nietubicz and K.O. Opalka, "Supersonic Wind Tunnel Measurements of Static and Magnus Aerodynamic Coefficients for Projectile Shapes with Tangent and Secant Ogive Noses," U.S. Army Ballistic Research Laboratory, Aberdeen Proving Ground, Maryland, ARBRL-MR-02991, February 1980. (AD A083297)*

15. *L.D. Kayser and W.B. Sturek, "Turbulent Boundary Layer Measurements on the Boattail Section of a Yawed, Spinning Projectile Shape at Mach 3.0," U.S. Army Ballistic Research Laboratory, Aberdeen Proving Ground, Maryland, ARBRL-MR-02880, November 1978. (AD A065355)*

adaptive grid technique first reported in Reference 2. The computational grid was generated algebraically for this axisymmetric configuration.

The marching step size and smoothing parameters employed for the SOC and SOCBT configurations were chosen according to the results presented in Reference 10. The marching step size at the nose tip was .01 calibers and was increased by 5% every 15 steps to a value of .03 calibers at the tail end of the projectile. Only fourth-order explicit smoothing was applied in these computations and was set equal to 5 times the step size. All SOC and SOCBT results were generated on a CDC 7600 computer with a speed of .00247 CPU sec/step/grid point. The total run times were approximately 30 minutes for a nonspin case and 60 minutes for a spin case.

Computations were performed by applying either the original Baldwin-Lomax turbulence model or the modified turbulence model over the entire length of the projectile.

1. Nonspin Case. For the case of zero spin, the initial appearance and downstream growth of the separated region on the lee side of the SOC and SOCBT projectiles can be clearly traced in Figures 5a and 5b. The circumferential location of crossflow separation is defined as the roll angle(s) at which the circumferential shear at the wall changes sign. The region of crossflow separation appears on the leeward side at an axial location of approximately 4 calibers and immediately begins to widen circumferentially around the projectile. The predicted axial position where crossflow separation initially appears and the size of the separated region is somewhat sensitive to whether the original or modified model is applied. It is also apparent that a major effect of the boattail is to cause this separated region to broaden further around the projectile.

The computed longitudinal surface pressure distributions on the wind and lee sides of the SOCBT at $\alpha = 6.3°$ are compared to experiment in Figure 6. The modified turbulence model was used for these computations. The agreement is quite good, most notably in the vicinities of discontinuities in stream wise surface curvature. The well-behaved longitudinal variation of surface pressures is used here as an indicator of the suitability of the marching step size and the smoothing parameters chosen.

The computed circumferential surface pressure distributions upstream of the boattail agree well with experiment with or without the modifications to the turbulence model, as was previously reported in Reference 6. In contrast, Figure 7 shows a comparison of circumferential surface pressure distribution near the end of the boattail configuration for the original and modified turbulence models compared with experimental measurement. The improvement in agreement due to the modified turbulence model is twofold. First, the agreement in trend on the leeward side is much improved; and second, the magnitude of the pressure on the windward side agrees within 1%.

The general effect of the modified turbulence model on longitudinal velocity profiles is shown in Figure 8. For zero spin, at roll angles where the turbulence scaling lengths are "clipped", a distinct deficit in the profile is consistently generated.

For zero spin, Figures 9a, 9b and 9c show longitudinal velocity profiles near the end of the boattail for the original and modified turbulence models compared to experiment. These three roll angles are included in the region of separation as defined in Figure 5b. At roll angles 120° and 150°, the modified turbulence model gives acceptable agreement with experiment and shows favorable trends compared to the original turbulence model. At roll angle 180°, however, the modified model gives a less favorable agreement with experiment. This implies that the modified turbulence model, as implemented here, does not provide an appropriate length scale near roll angle 180°.

Very little difference in the predicted aerodynamic forces and moments was observed using either the original or modified turbulence model for the nonspinning shell.

2. Spin Case. A more sensitive test of the performance of the modified turbulence model is the prediction of the Magnus effect for a spinning shell. Application of the modified turbulence model to the spin case, it was hoped, would follow directly from the case of zero spin. However, initial results indicated that the cutoff distance for y_{max} (1.8 times the value on the windward side) was too strict for the case of spin. By relaxing the cutoff distance to 3.0 times the value on the windward side, better agreement was obtained between computation and experiment.

The development of Magnus force (sign convention given in Figure 10) over the spinning SOCBT projectile is shown in Figure 11. Both the original and modified turbulence models yield good agreement with experiment. If, when applying the modified model, the cutoff distance factor for y_{max} had been set to 1.8 rather than 3.0, the Magnus force would have been overpredicted by 20%.

The effect of the modified turbulence model on the longitudinal velocity profiles for the spin case compared to experiment is shown in Figures 12a thru 12c. As for the nonspin case, the modified turbulence model causes a velocity deficit compared to the original model. At roll angle 210°, the modified model agrees substantially better with experiment than the original model. At roll angles 120° and 240°, the overall agreement is satisfactory. At roll angle 180° (not shown here) the agreement is less favorable.

B. Long L/D Finned Body Configurations

The results for long L/D finned body configurations are presented in two parts. First, results are presented for smooth axisymmetric forebodies of a shape typical of kinetic energy penetrators and comparisons made with wind tunnel data. Results are then presented for a complete finned body configuration (forebody plus fins) and comparisons made with inviscid code predictions and with free-flight range data.

1. Forebodies. Computations have been performed using the PNS technique to examine the effect of length to diameter ratio (L/D) on the aerodynamics of axisymmetric kinetic energy penetrator forebodies and the results compared

with wind tunnel data.[16] Figure 13 shows the forebody shape as modeled in the wind tunnel tests. The primary difference between the computational model and the wind tunnel model is that the small step decrease in diameter over the aft portion of the wind tunnel model forebody has been neglected in the computational model. This difference, it is felt, should not have a significant effect on the prediction of pitch-plane aerodynamic coefficients.

The gridding for these calculations consisted of 60 points from the body to the shock and 37 points circumferentially around the body in the half plane of symmetry. The circumferential gridding was chosen after performing a study examining the effect of circumferential resolution on an eight degree cone-cylinder configuration, for free-flight conditions, Mach 4, and free stream Reynold's number (based on body diameter) of 3.2 million. Figure 14 shows the development of the normal force over the body for varying degrees of circumferential resolution. While 19 circumferential points may be adequate for calculations of short L/D bodies, such as shell configurations, long L/D bodies require more resolution for accurate solution. Circumferential resolution of 37 points and above appears to give adequate resolution for these long axisymmetric bodies.

Results are presented here for Mach numbers of 4 and 5, 2° angle of attack, and turbulent flow conditions over the body. Free stream conditions corresponding to the wind tunnel test conditions have been used. Constant wall temperature boundary conditions, (wall temperature = 294K) were also applied at the body surface.

After obtaining the initial plane of data from the conical marching procedure at a position 0.53 calibers from the nose, the solution was marched down the body using a step size of .021 calibers, The spacing from the wall to the first point above the wall was adjusted so that the first point above the wall was within the laminar sublayer; the boundary layer coordinate, y^+, was maintained less than five.

Figure 15 and 16 show the development of the normal force and pitching moment (referenced to the projectile nose) over the body at Mach 4 and 2° angle of attack. Good agreement is seen between the computation and the experiment at 25 calibers. Scatter in the experimental data at 35 calibers is evident, emphasizing the difficulties in performing such a test for these long bodies.

Similar agreement is seen for the results at Mach 5 and 2° angle of attack, shown in Figures 17 and 18. Again, scatter in the experimental data is evident at the higher L/D's.

Figure 19 shows the effect of Mach number and Reynold's number on the development of normal force over the body. Here, the results discussed above for Mach 4 (Re = 0.41 million, based on body diameter) and Mach 5 (Re = 0.54 million) are shown along with a free-flight calculation at Mach 4 (Re =

---

[16] *F. Brandon, "private communications," unpublished wind tunnel data, U.S. Army Ballistic Research Laboratory, Aberdeen Proving Ground, Maryland*

2.2 million). Evidently in this Mach number and Reynold's number regime, both Mach number and Reynold's number are significant parameters to be simulated. While computations can, to some degree, simulate both Reynold's and Mach numbers, such simulation is difficult in the wind tunnel and suggests the need to scale the wind tunnel data to free flight conditions for these long L/D bodies.

The effect of length to diameter ratio on the development of normal force can also be deduced from Figure 19. For shorter bodies, L/D < 12, the development of normal force increases significantly with L/D, and the variation is due almost purely to inviscid effects. For larger L/D's, the variation of normal force with L/D is smaller, and is dominated primarily by viscous effects. For length to diameter ratios greater than about 20, the normal force, in the range of Reynold's numbers of interest, shows a small increase due to the thickening of the boundary layer.

2. Finned Projectile Configuration. The finned body configuration for which calculations have been performed closely resembles the M735 Army projectile. The modeled finned body configuration is characterized by a conical nose section joined to a smooth cylindrical main body with six symmetrical swept fins attached to the aft section of the projectile. Figure 20 depicts the basic dimensions of this configuration. The actual projectile differs from the modeled projectile in that the actual projectile has: (1) circumferential grooves over much of the cylindrical portion of the body to prevent the sabot from sliding off the body in the gun tube; (2) fins which have a nonsymmetrical sectional geometry to induce roll, and (3) a slightly rounded nose. Modeling the projectile with a sharp nose and symmetrical fin section are not the result of inherent limitations of the computational model, but rather a matter of convenience for these initial calculations. While modeling of the sabot grooves may be possible using surface blowing, wind tunnel results have shown that such grooves have almost no effect on the value of normal force and pitching moment. These grooves do, however, have a noticeable effect on drag, particularly at higher angle of attack.[16]

A shadowgraph of the actual projectile in flight at Mach 4.3 is shown in Figure 21 and displays some of the relevant features of the flow field; a bow shock wave emanating from the nose of the projectile, shocks at the leading edge of the fins, expansion waves at the cone-cylinder junction, and a boundary layer which increases along the body.

Results are presented here for Mach number of 3, 4 and 5, 2° angle of attack, and turbulent flow conditions over the body. Atmospheric flight conditions were simulated by maintaining the body temperature at the free stream value of 294K. Calculations were made with two of the fins oriented vertically, enabling a half plane of symmetry to be applied.

An initial plane of data was generated using the conical step back procedure at position 0.36 calibers from the nose. The solution was then marched down the body to a position near the beginning of the fins using a step size of 0.014 calibers, 60 points from the body to the shock, and 121 points circumferentially about the body in the half plane of symmetry. Over the cone-cylinder portion of the body only fourth-order explicit smoothing was used. Spacing from the wall to the first point above the wall was again maintained so that at least one point was in the laminar sublayer.

Once on the finned portion of the body, the grid was obtained through the use of an elliptic grid generator.[7] Points on the body surface were clustered near the leading edge of the fins, as shown in Figure 22. Figures 23a and b show a cross section of the grid on the finned portion of the body at an axial location on X/D = 13.2. Grid points are clustered near the body to resolve the boundary layer.

Substantial difficulty had been encountered in previous calculations[10] in marching the solution over the finned portion of the body. Prior solutions were only obtained using large amounts of smoothing and a coarse grid which did not properly resolve the viscous layer over the fins. For the current set of calculations, a small fillet was applied axially from the cone-cylinder onto the leading edge of the fins. The fillet, of constant radius, began 0.07 calibers in front of the fins and ended at a position where it became tangent to the leading edge of the fins. This allowed a solution to be obtained with significantly improved resolution of the boundary layer over the fins and with only 5% of the previously applied smoothing. Current values of smoothing[17] used for these calculations are shown in Table 1. In marching the solution over the finned portion of the body, the step size was reduced from 0.014 calibers to 0.0072 calibers.

Table 1. Smoothing Parameters for Finned Body Calculations

SMOOTHING PARAMETERS	CONE-CYLINDER	FINS M = 3	 M = 4	 M = 5
SMU	0.015	0.05	0.05	0.025
SMUIM	0.	0.1	0.1	0.05
EPSA	0.	0.05	0.05	0.025
EPSB	0.	0.05	0.05	0.025

Figure 24 displays the pressure along the body on the wind and lee sides and at a roll angle of 90° at Mach 4. A sharp rise in pressure on the leading edge of the wind and lee fins is seen, followed by a sharp drop at the axial location where the fin reaches its maximum span. Over the finned portion of the body the ϕ = 90° line shows a jump in pressure due to the interaction of the shocks from the adjacent fins. It is interesting to note that, due to the significant reduction in smoothing required to generate a solution, the pressure predicted on the leading edge of the fins is smaller than that

---

17. D.S. Chaussee, J.L. Patterson, P. Kutler, T. Pulliam and J.L. Steger, "A Numerical Simulation of Hypersonic Viscous Flow Over Arbitrary Geometries at High Angle of Attack," AIAA Paper No. 81-0050, January 1981.

previously calculated, and the jump in pressure due to the interaction of the shocks is more pronounced.

Figure 25 shows the development of the normal force coefficient over the body. The normal force coefficient shows a moderate contribution due to the conical nose and cylindrical portion of the body and a larger contribution due to the finned portion of the body. In this figure comparison is made with results obtained with the NSWC inviscid code (SWINT)[18] and range data[19] for the actual projectile configuration. The SWINT code solves the Euler equations for the supersonic flow over bodies with fins and/or wings and for the external flow about bodies with inlets. The code makes use of the thin fin approximation, collapsing each fin along a single radial plane in the grid. The fin leading edges must be sharp and cannot extend beyond the bow shock. Variations in the fin cross section geometry can be accounted for in the code by the application of appropriate local analysis such as shock compression and Prandtl-Meyer expansion theories, though this has not been utilized in the computations presented here. For the current SWINT computations, the fins have been modeled as a flat plate of zero thickness.

Development of the normal force as predicted by the PNS and SWINT codes compare well, particularly over the cone-cylinder portion of the body. For forebodies with L/D's greater than the current configuration, differences in the viscous (PNS) and inviscid (SWINT) code predictions can be expected due to viscous effects. (Figure 13, previously presented, shows little effect of Reynold's number at L/D's less than about 12.) Over the finned portion of the body, slightly more lift is being predicted in PNS computations. Good agreement between the total value of normal force for both procedures is seen compared with the range data.

The variation of the predicted values of the slope of the normal force and pitching moment coefficients with Mach number are compared with the values predicted by the SWINT code and with range data in Figures 26 and 27. (Pitching moment here has been referenced to the center of gravity shown in Figure 20.) The PNS code is seen to predict slightly larger values of normal force and pitching moment compared with the range data and inviscid code predictions at Mach 3 and 4. PNS and inviscid code predictions agree very well at Mach 5. Differences in agreement between the PNS and inviscid code predictions at Mach 3 and 4 occur almost entirely over the finned portion of the body, though at this point such differences can not be attributed entirely to viscous effects. It should be noted again that the exact fin geometry has not been modeled in either the PNS or SWINT computations. Efforts to model the fin geometry as closely as possible are underway.

---

[18] *A.B. Wardlaw, Jr., F.P. Baltakis, J.M. Solomon and L.B. Hackerman, "An Inviscid Computational Method for Tactical Missile Configurations," NSWC TR 81-457.*

[19] *Unpublished range data, U.S. Army Ballistic Research Laboratory, Aberdeen Proving Ground, Maryland.*

An additional calculation at Mach 3 was run over the finned portion of the body using 181 points circumferentially in the half plane. Variations in the predicted values of normal force between the computations with 121 and 181 circumferential points was less than a tenth of a percent. Comparisons of the circumferential pressure distribution at several axial stations showed very little difference. This result established that the current circumferential resolution of 121 points was adequate.

IV. CONCLUSIONS

A. Computations at Moderate Angle of Attack

Computational results for SOC and SOCBT shell configurations with and without spin have been generated at angle of attack 6.3°. One set of results employs a modification to the Baldwin-Lomax turbulence model; the other set of results uses the model in its original form. Both sets of results were compared to available wind tunnel data in order to assess the predictive capability for flows with crossflow separation at this angle of attack.

For the case of zero spin, the modified turbulence model significantly improved the agreement of circumferential pressure distributions where crossflow separation is present. Velocity profile comparisons on the boattail were generally improved, with the modified model consistently generating a velocity deficit compared to the original model. The variation between the predicted pitch plane and drag coefficients using the original and modified turbulence models was very small, and the coefficients were in good agreement with experiment.

For the case with spin (PD/V = .19), the modified turbulence model had to be relaxed to obtain good agreement with experimental Magnus force and velocity profile data. The need to allow larger scaling lengths for the case of spin is evidence that characteristic differences may exist in the turbulence modeling requirements for spinning and nonspinning bodies with crossflow separation.

B. Computations for Long L/D Finned Body Configurations

Results of the computations for the long L/D axisymmetric forebodies show good agreement with the wind tunnel data for pitch-plane aerodynamic coefficients at L/D's of 20 and 25. Scatter in the experimental data at higher L/D's makes comparisons difficult. The computations demonstrate the importance of considering viscous effects for these long bodies.

Computations were performed for the finned body configuration and show encouraging agreement with range data and inviscid code predictions. Computations were obtained with significantly improved resolution of the viscous layer on the fins and without the need for large amounts of smoothing over this portion of the body, compared to results previously obtained.

ACKNOWLEDGMENT

The authors wish to thank Dr. Lewis B. Schiff, NASA Ames Research Center, for his valuable discussions and assistance during the important late stages of the project.

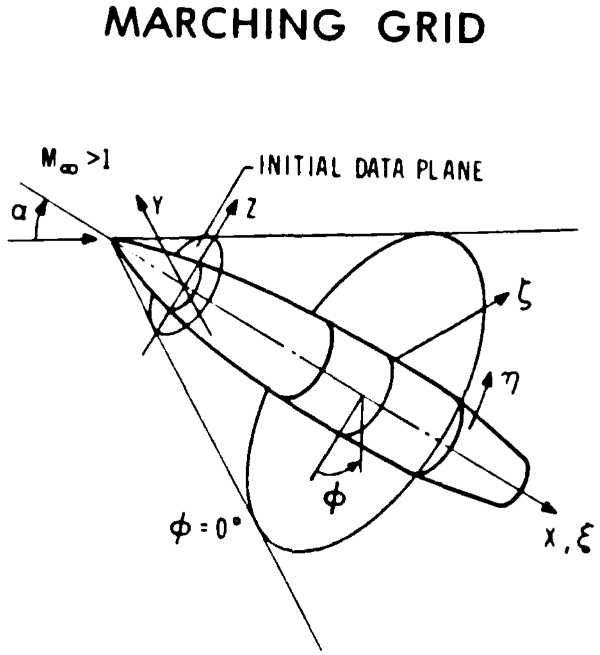

Figure 1. Grid Coordinates and Notation

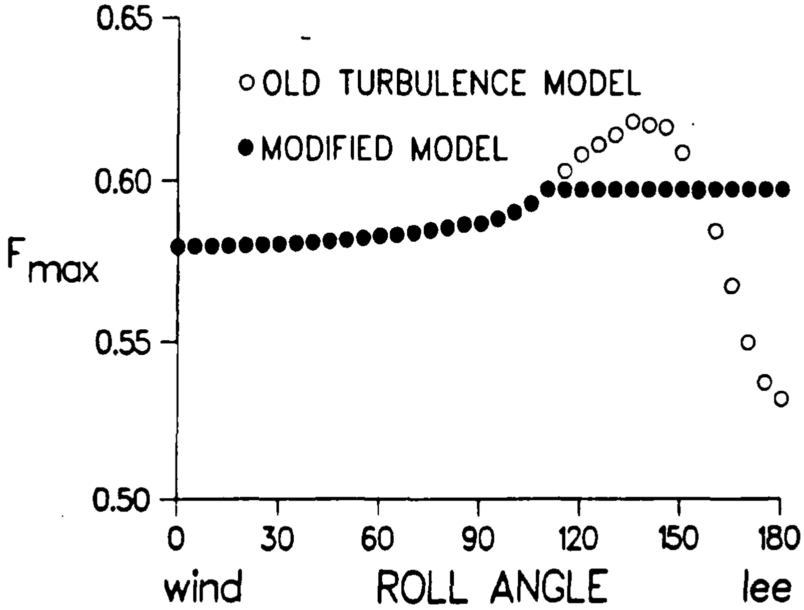

Figure 2. Circumferential Variation of F_{max} for SOC and SOCBT Configurations; $M = 3$, $\alpha = 6.3°$, $PD/V = 0$, $Re = 2.13 \times 10^7/m$, $X/D = 4.29$

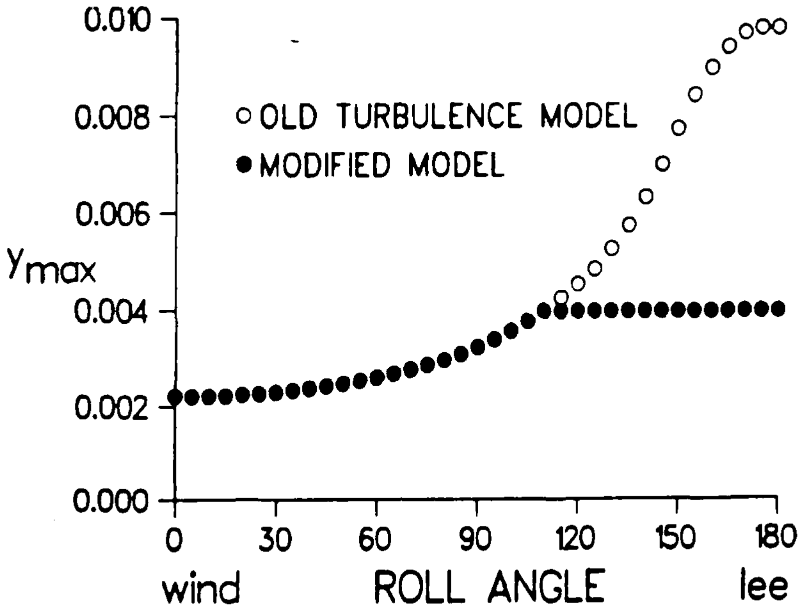

Figure 3. Circumferential Variation of y_{max} for SOC and SOCBT Configurations; M = 3, $\alpha = 6.3°$, PD/V = 0, Re = 2.13×10^7/m, X/D = 4.29

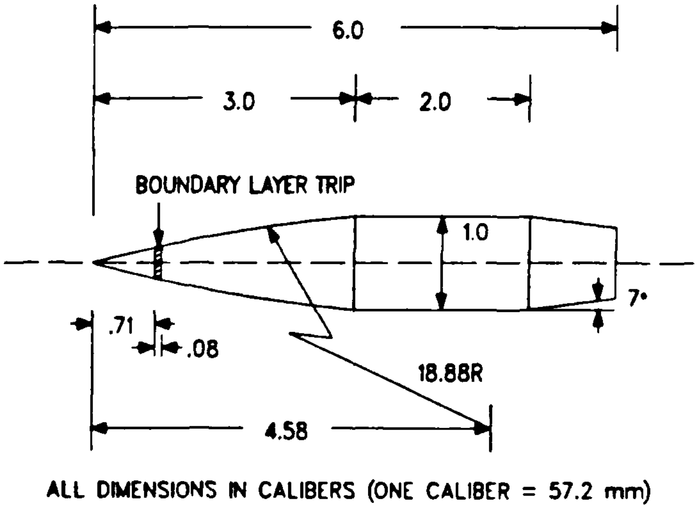

Figure 4. Secant Ogive-Cylinder-Boattail (SOCBT) Model Configuration

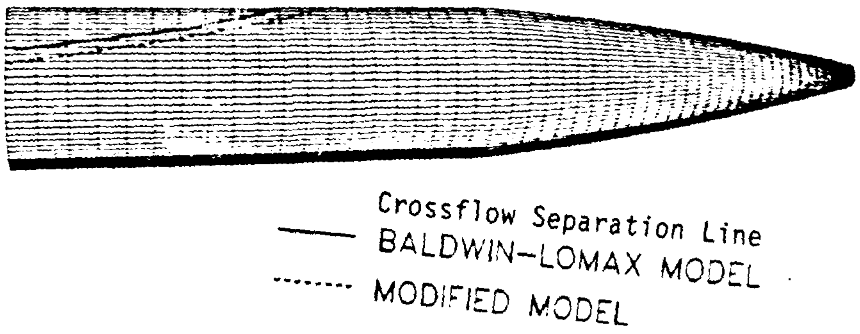

Figure 5a. Region of Crossflow Separation for SOC Configuration, $M = 3$, $\alpha = 6.3°$, $PD/V = 0$, $Re = 2.13 \times 10^7/m$

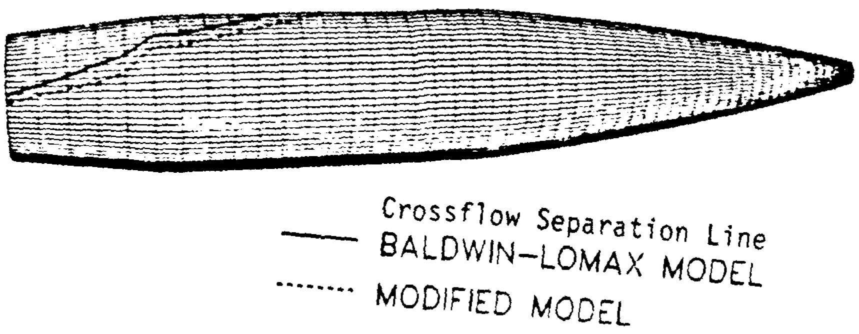

b. SOCBT

Figure 5b. Region of Crossflow Separation for SOCBT Configuration; $M = 3$, $\alpha = 6.3°$, $PD/V = 0$, $Re = 2.13 \times 10^7/m$

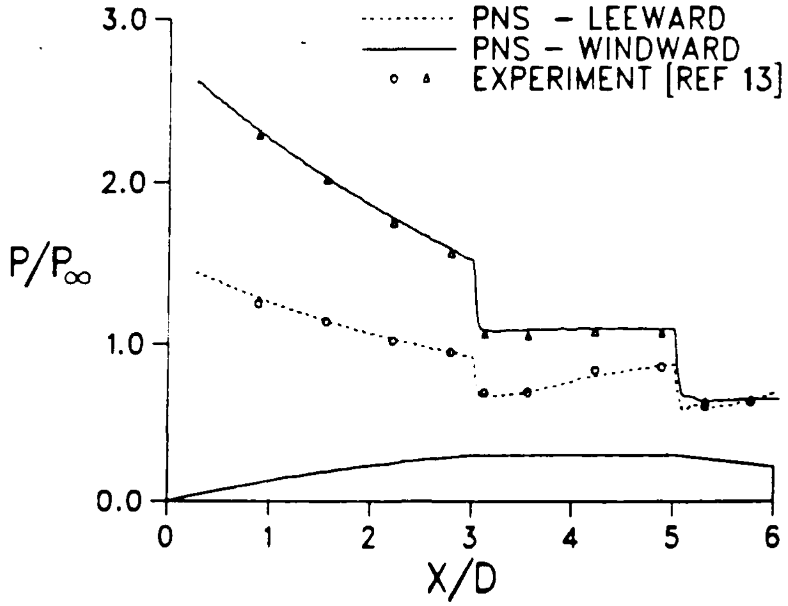

Figure 6. Longitudinal Surface Pressure Distribution for SOCBT Configuration; M = 3, α = 6.3°, PD/V = 0, Re = 2.13 × 10^7/m

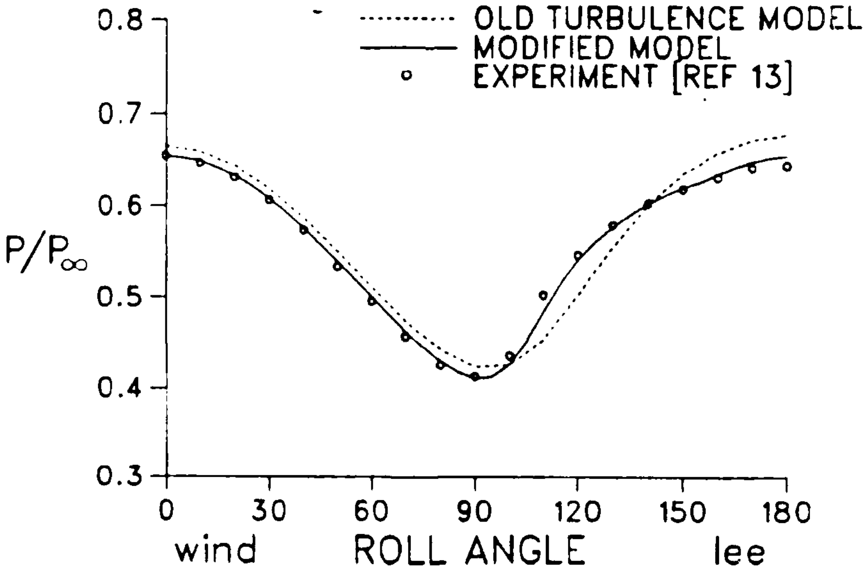

Figure 7. Circumferential Surface Pressure Distribution for SOCBT Configuration; M = 3, α = 6.3°, PD/V = 0, Re = 2.13 × 10^7/m, X/D = 5.77

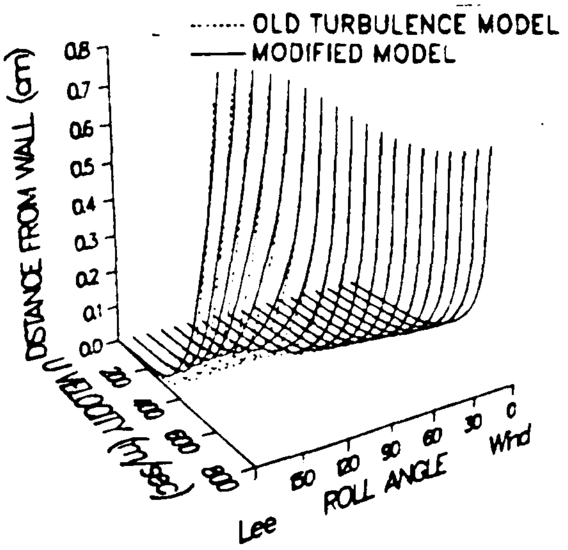

Figure 8. Longitudinal Velocity Profiles for SOCBT Configuration; M = 3, α = 6.3°, PD/V = 0, Re = 2.13 × 10^7/m, X/D = 5.67

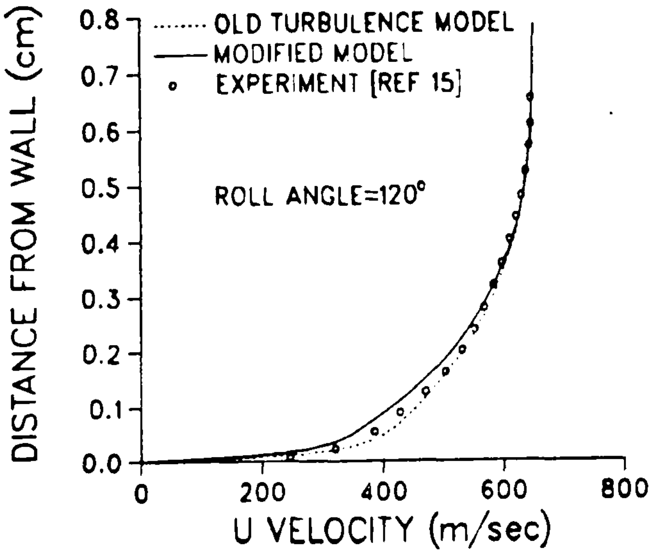

Figure 9a. Longitudinal Velocity Profile for SOCBT Configuration; M = 3, α = 6.3°, PD/V = 0, Re = 2.13 × 10^7/m, X/D = 5.67, ϕ = 120°

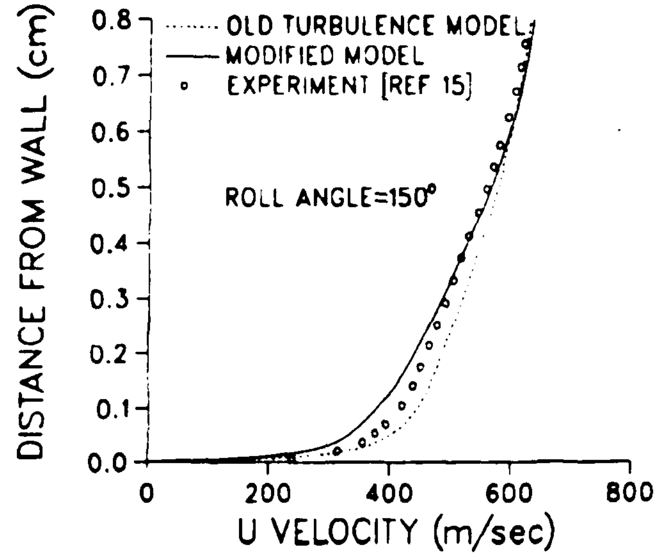

Figure 9b. Longitudinal Velocity Profile for SOCBT Configuration; M = 3, $\alpha = 6.3°$, PD/V = 0, Re = 2.13×10^7/m, X/D = 5.67, $\phi = 150°$

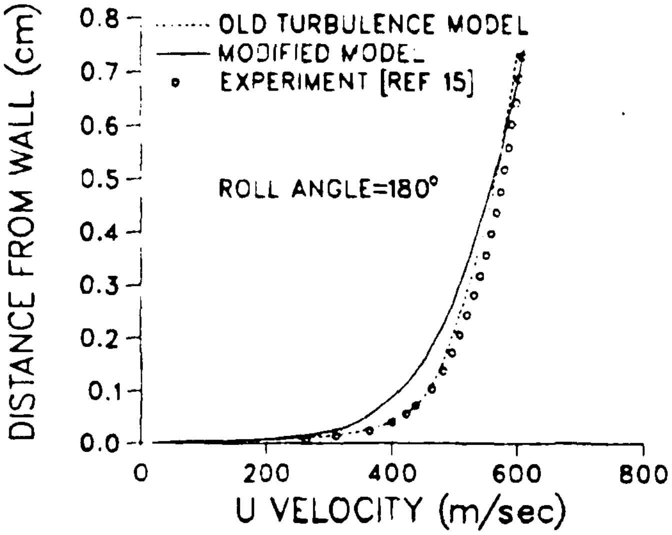

Figure 9c. Longitudinal Velocity Profile for SOCBT Configuration; M = 3, $\alpha = 6.3°$, PD/V = 0, Re = 2.13×10^7/m, X/D = 5.67, $\phi = 180°$

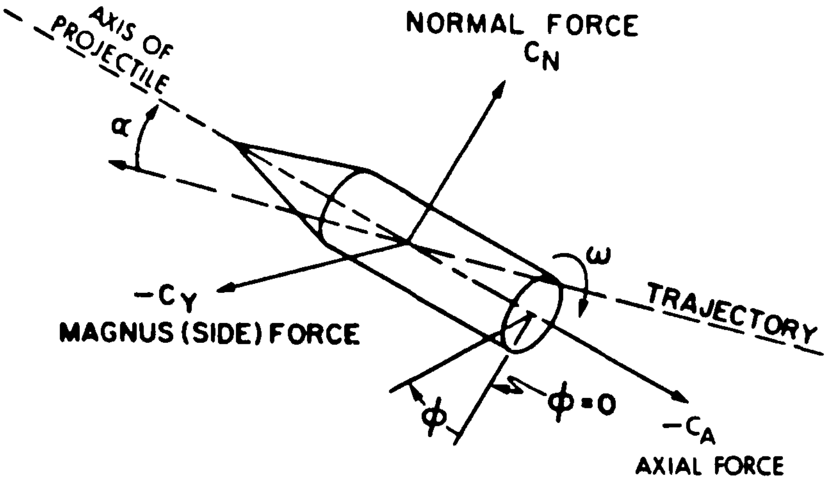

Figure 10. Sign Convention for Spin and Aerodynamic Force Coefficients

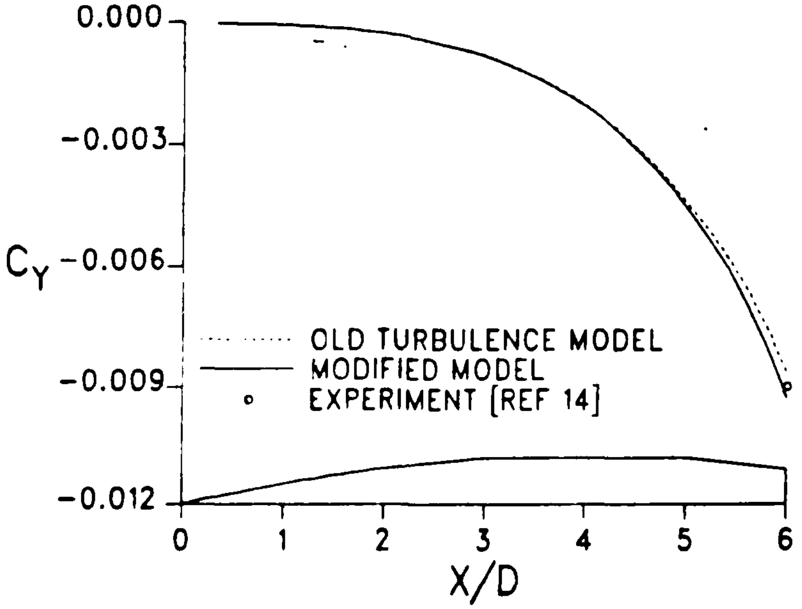

Figure 11. Total Magnus Force Coefficient Developing over SOCBT Configuration; $M = 3$, $\alpha = 6.3°$, $PD/V = .19$, $Re = 2.13 \times 10^7/m$

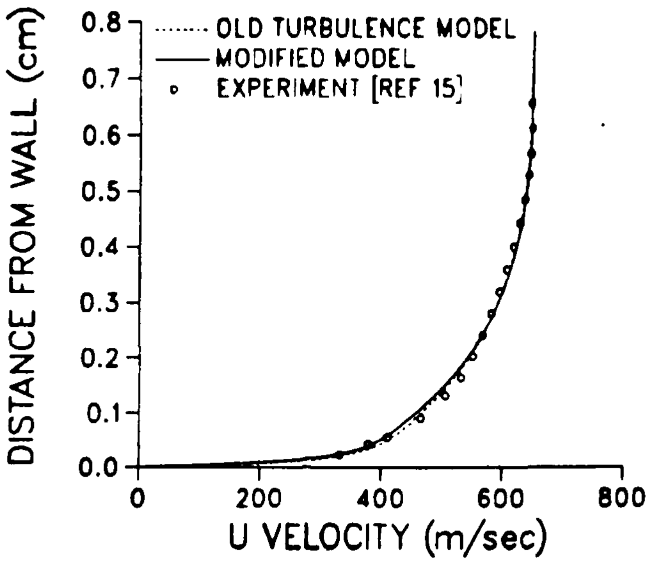

Figure 12a. Longitudinal Velocity Profile for SOCBT Configuration; M = 3, $\alpha = 6.3°$, PD/V = .19, Re = 2.13×10^7/m, X/D = 5.67, $\phi = 120°$

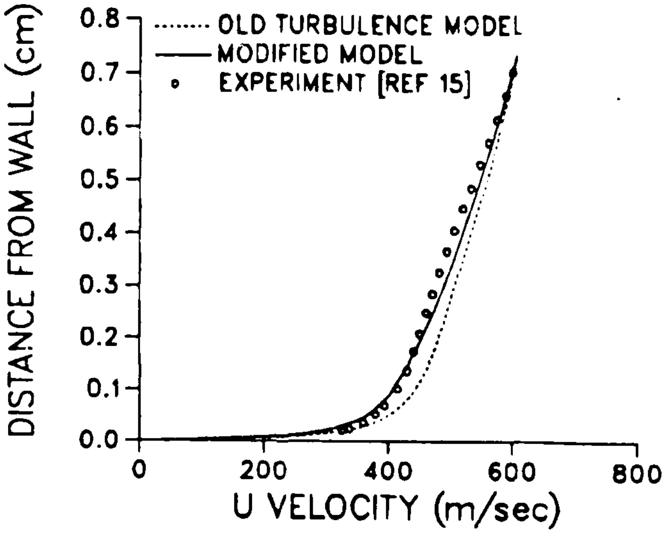

Figure 12b. Longitudinal Velocity Profile for SOCBT Configuration; M = 3, $\alpha = 6.3°$, PD/V = .19, Re = 2.13×10^7/m, X/D = 5.67, $\phi = 210°$

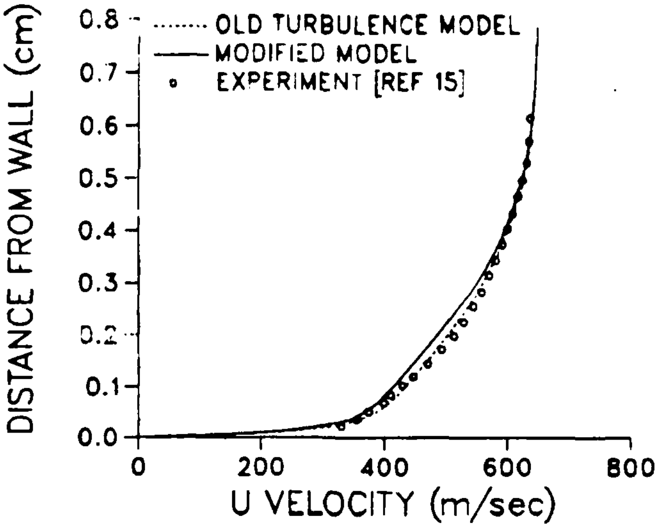

Figure 12c. Longitudinal Velocity Profile for SOCBT Configuration; M = 3, $\alpha = 6.3°$, PD/V = .19, Re = 2.13×10^7/m, X/D = 5.67, $\varphi = 240°$

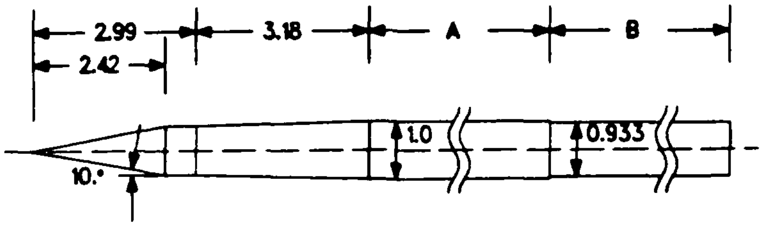

BODY	A	B
20 Cal	6.17	8.23
25 Cal	9.21	10.20
30 Cal	12.22	12.17
35 Cal	15.23	14.17

ALL DIMENSIONS IN CALIBERS
ONE CALIBER = 23.8 mm

Figure 13. Forebody Configuration

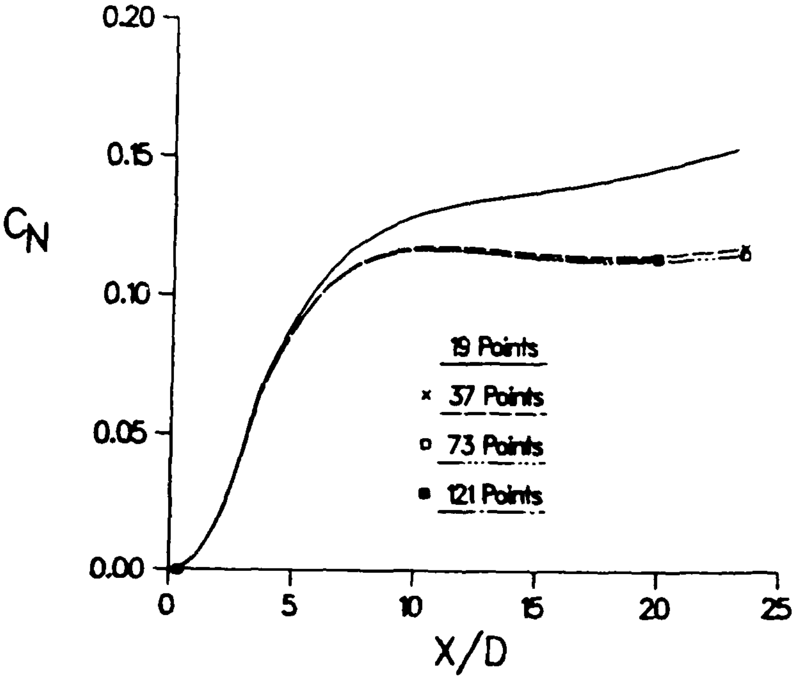

Figure 14. Development of Normal Force Coefficient along Body for Varying Circumferential Resolution, M = 4, $\alpha = 2°$, $Re_D = 3.2 \times 10^6$

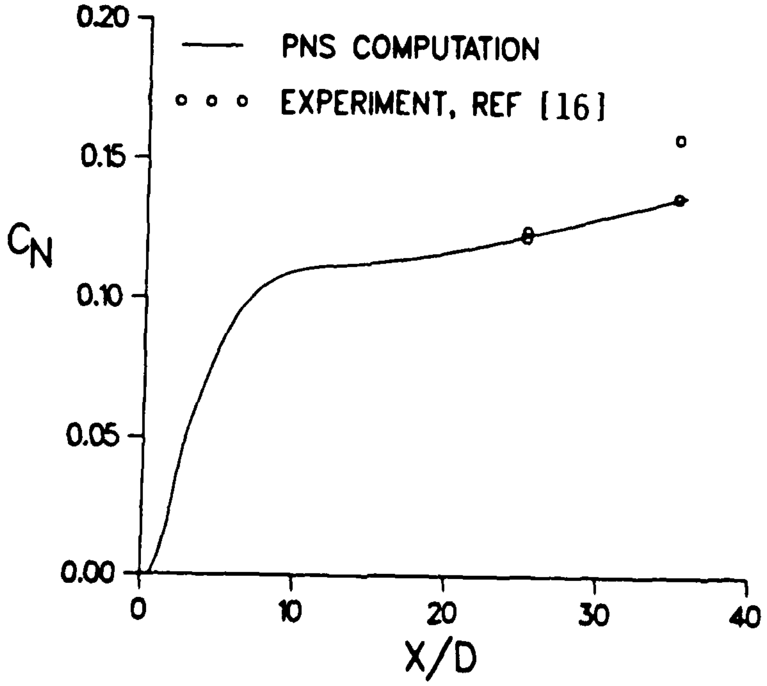

Figure 15. Development of Normal Force Coefficient along Body, M = 4, $\alpha = 2°$, $Re_D = 0.41 \times 10^6$

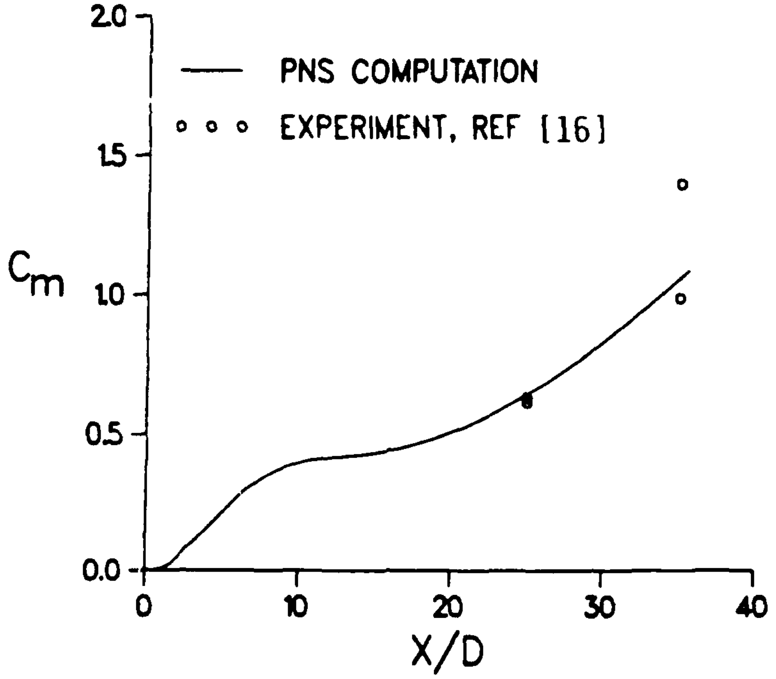

Figure 16. Development of Pitching Moment Coefficient along Body, M = 4, $\alpha = 2°$, $Re_D = 0.41 \times 10^6$

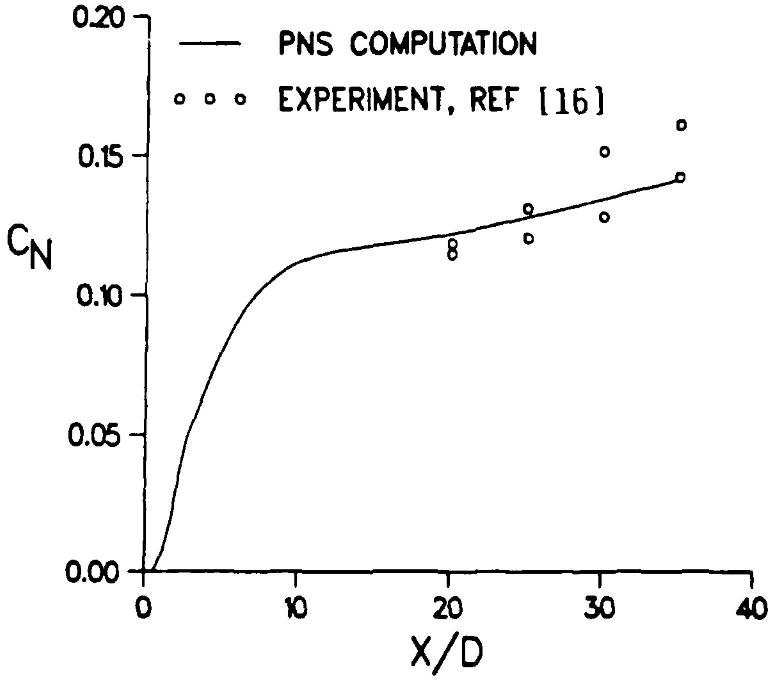

Figure 17. Development of Normal Force Coefficient along Body, M = 5, $\alpha = 2°$, $Re_D = 0.54 \times 10^6$

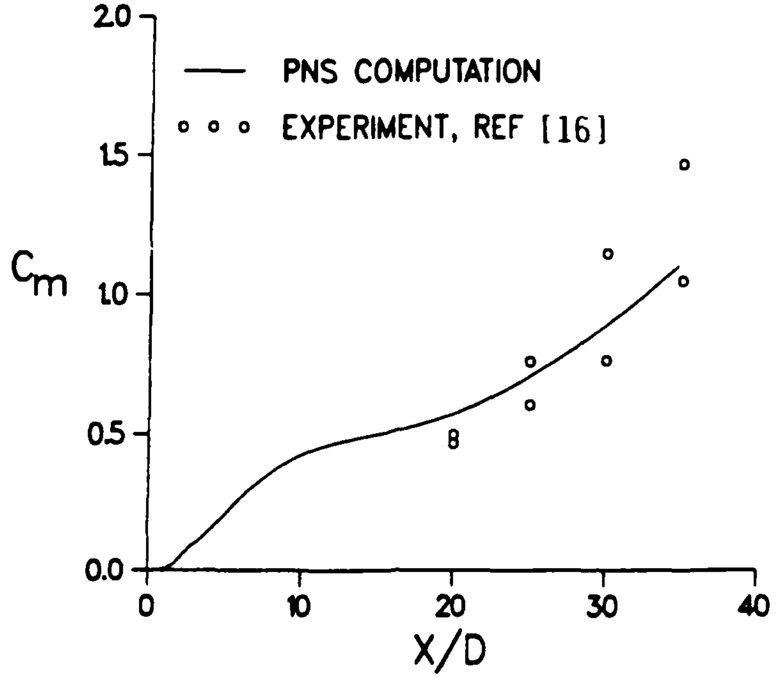

Figure 18. Development of Pitching Moment Coefficient along Body, M = 5, $\alpha = 2°$, $Re_D = 0.54 \times 10^6$

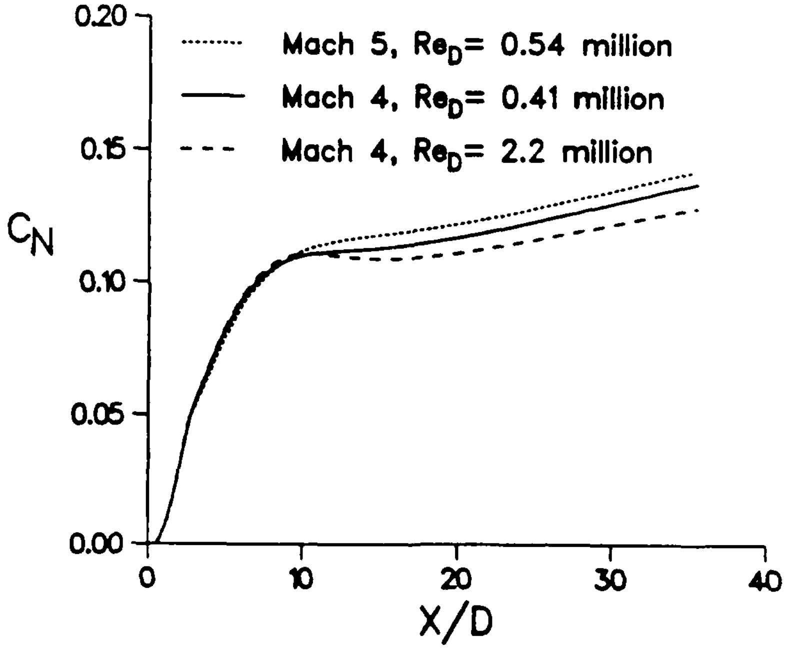

Figure 19. Development of Normal Force Coefficient over Long L/D Axisymmetric Body, Effect of Mach and Reynold's Numbers, $\alpha = 2°$

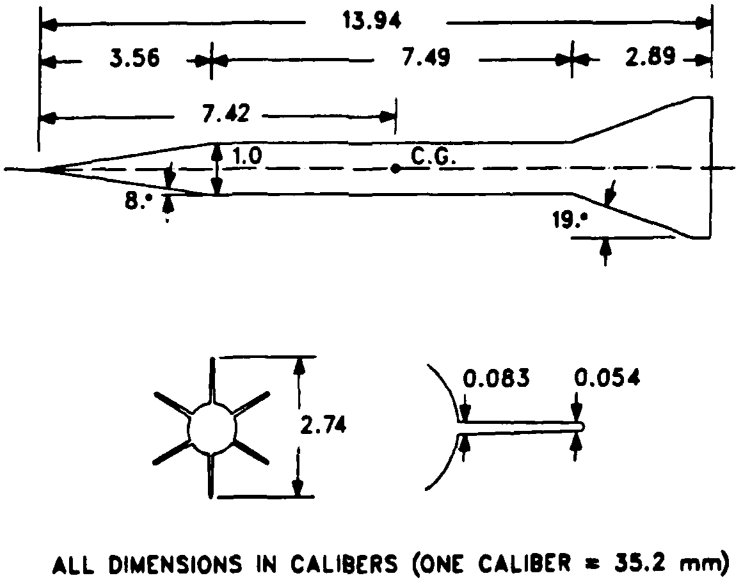

Figure 20. Finned Projectile Configuration

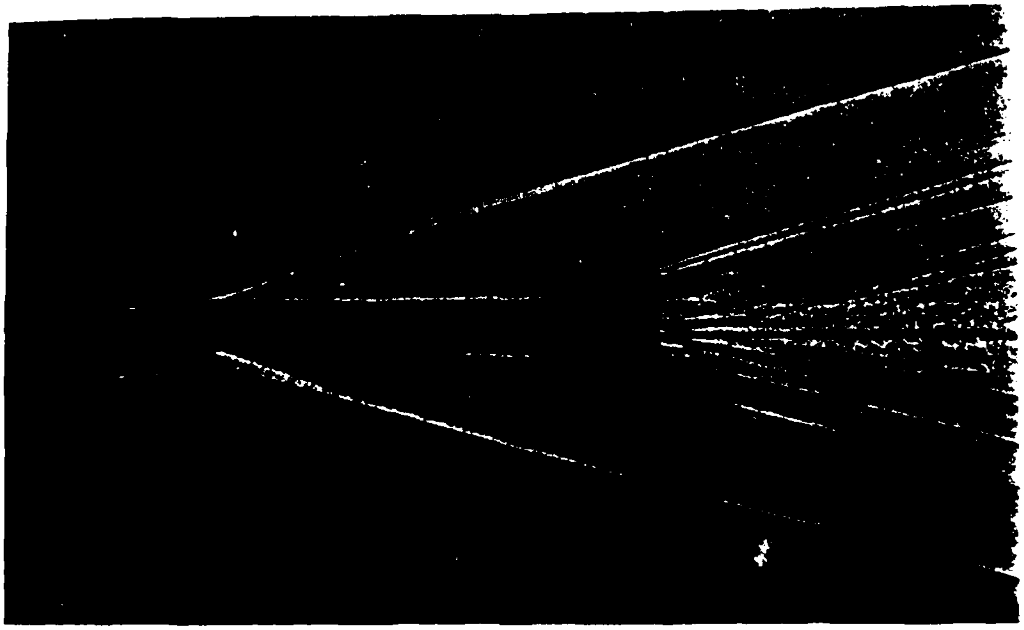

Figure 21. Shadowgraph of M735 in Flight

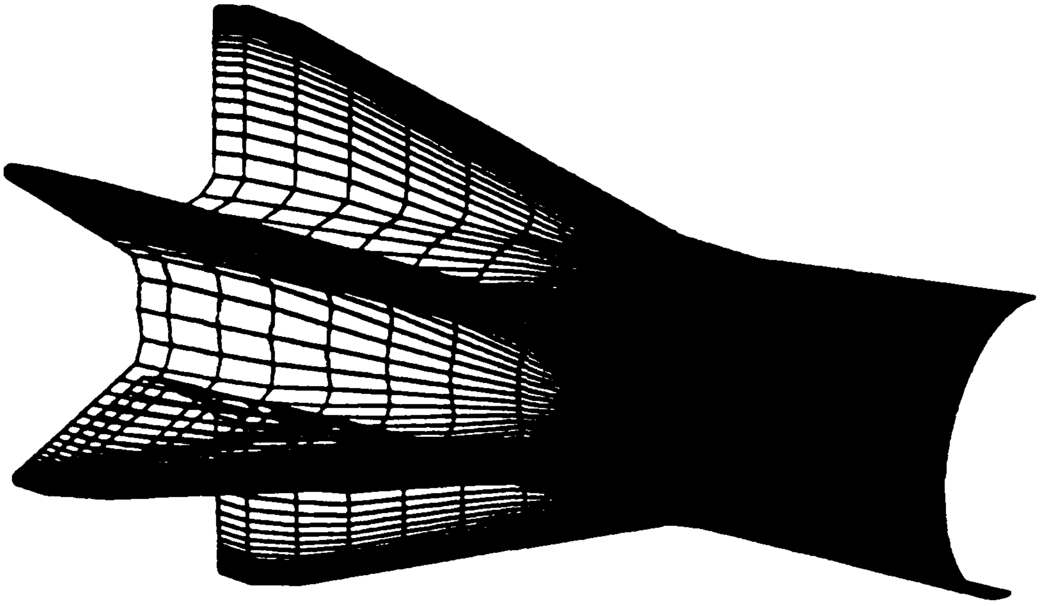

Figure 22. Grid on Body Surface on Finned Portion of Projectile

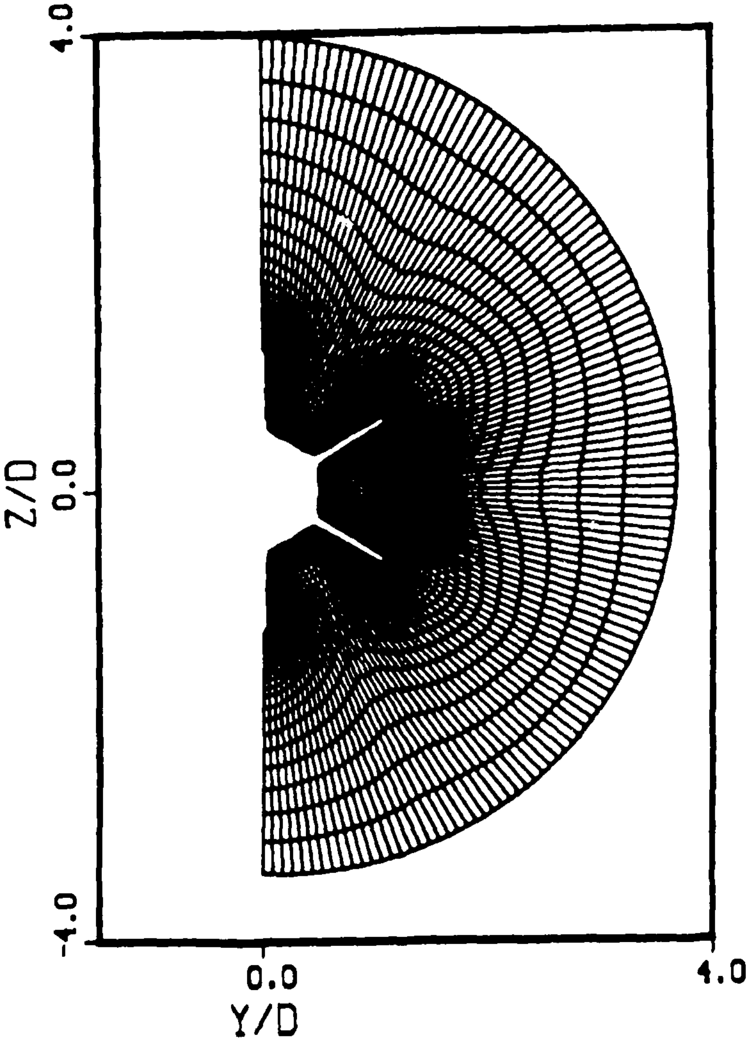

Figure 23a. Cross Section of Grid at X/D = 13.2, Half Plane Grid

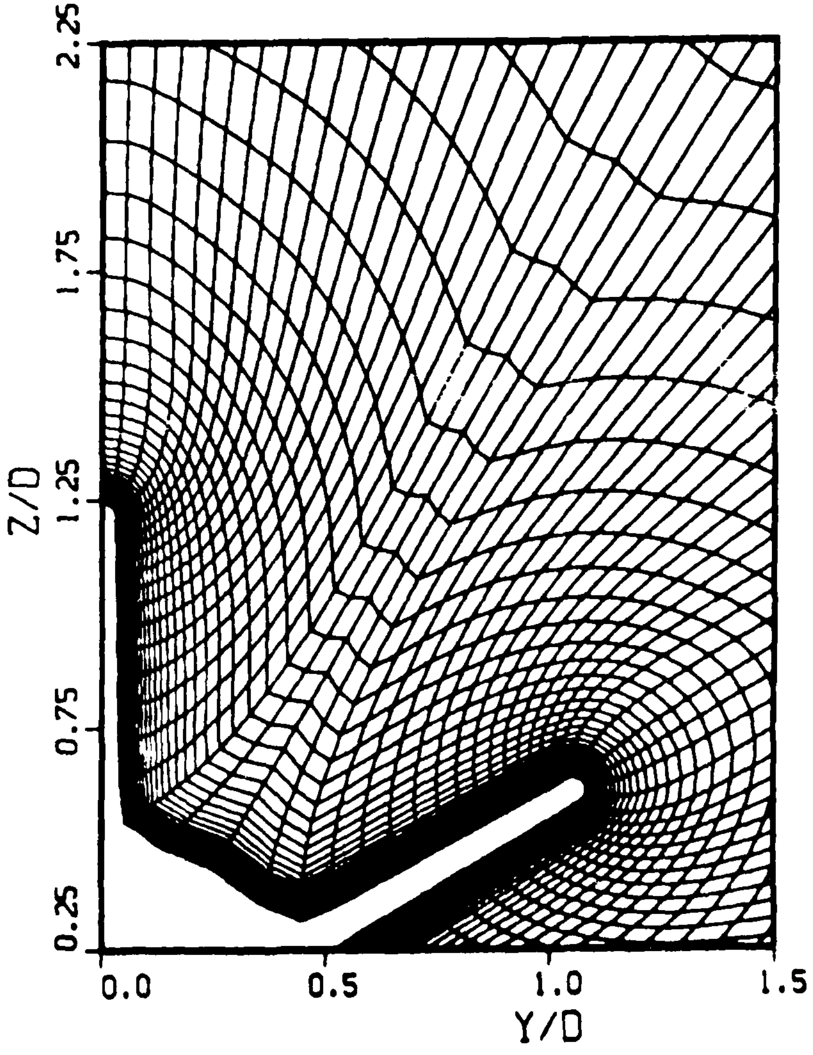

Figure 23b. Cross Section of Grid at X/D = 13.2, Close-Up of Grid Near Body

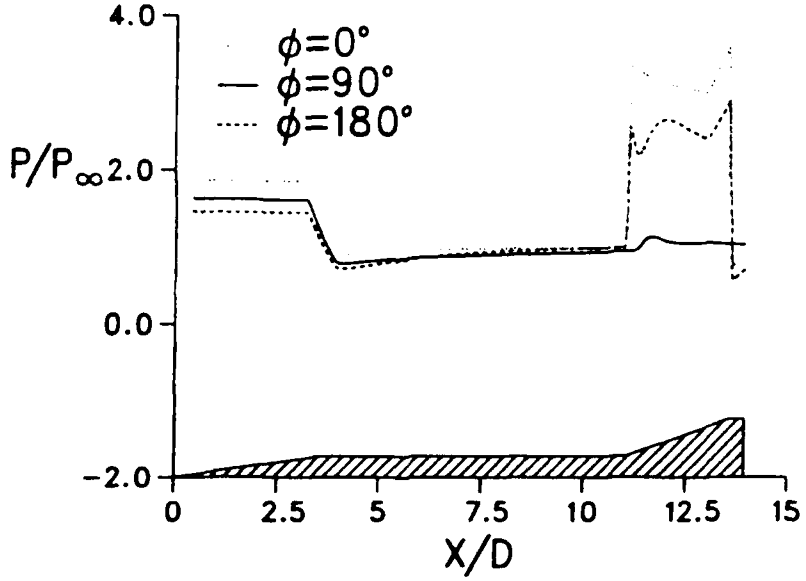

Figure 24. Axial Pressure Distribution at ϕ = 0 , 90° and 180°, M = 4, α = 2°, Re_D = 3.2 × 10^6

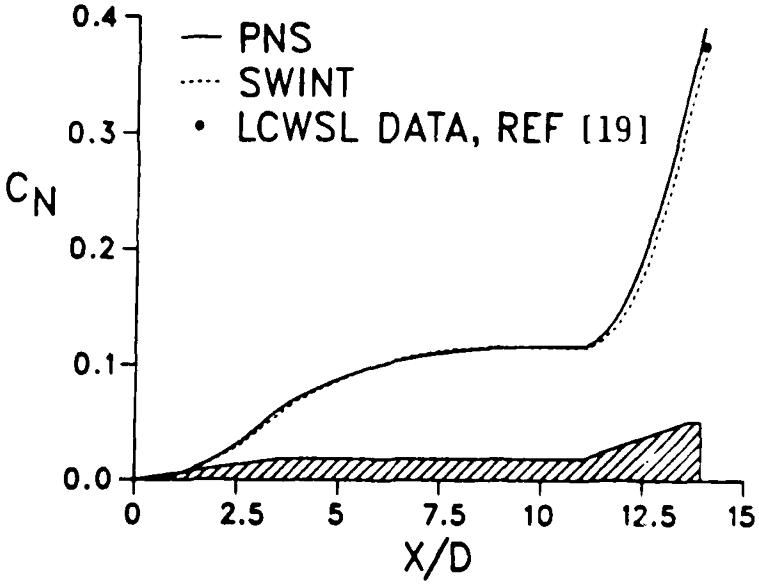

Figure 25. Development of Normal Force Coefficient along the Body, M = 4, α = 2°, Re_D, = 3.2 × 10^6

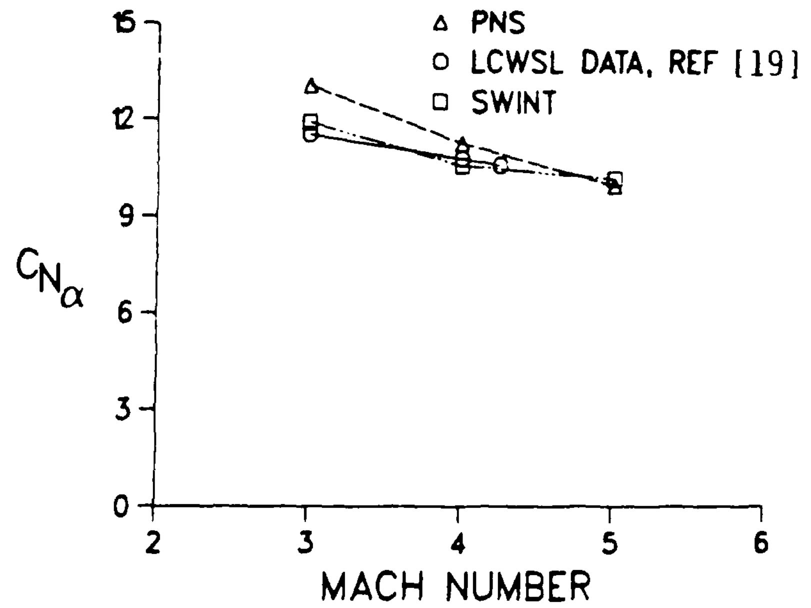

Figure 26. Zero-Degree Slope of the Normal Force Coefficient versus Mach Number

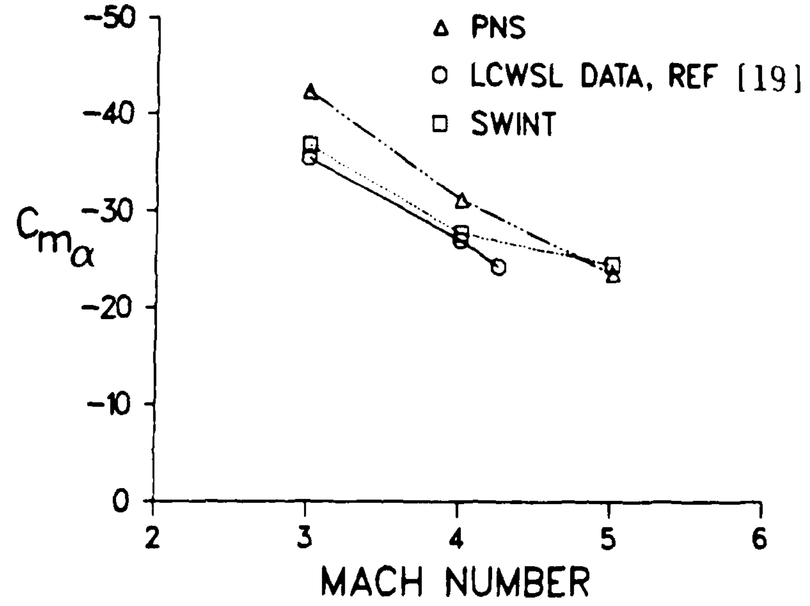

Figure 27. Zero-Degree Slope of the Pitching Moment Coefficient versus Mach Number

REFERENCES

1. W. B. Sturek, D. C. Mylin, and C. C. Bush, "Computational Parametric Study of the Aerodynamics of Spinning Bodies at Supersonic Speeds," U.S. Army Ballistic Research Laboratory, Aberdeen Proving Ground, Maryland, ARBRL-TR-02358, August 1981. (AD A106074)

2. W. B. Sturek and L. B. Schiff, "Computations of the Magnus Effect for Slender Bodies in Supersonic Flow," U.S. Army Ballistic Research Laboratory, Aberdeen Proving Ground, Maryland, ARBRL-TR-02384, December 1981. (AD A110016)

3. L. B. Schiff and W. B. Sturek, "Numerical Simulation of Steady Supersonic Flow Over an Ogive Cylinder Boattail Body," U.S. Army Ballistic Research Laboratory, Aberdeen Proving Ground, Maryland, ARBRL-TR-02363, September 1981. (AD A106060)

4. M. McWerter, R. W. Noack, and W. L. Oberkampf, "Evaluation of Inviscid/Boundary Layer and Parabolized Navier-Stokes Solutions for Design of Reentry Vehicles," AIAA Paper No. 84-0486, 22nd Aerospace Sciences Meeting, January 1984.

5. B. S. Baldwin and H. Lomax, "Thin Layer Approximation and Algebraic Model for Separated Turbulent Flows," AIAA Paper No. 78-257, 16th Aerospace Sciences Meeting, January 1978.

6. D. Degani and L. B. Schiff, "Computation of Supersonic Viscous Flows Around Pointed Bodies at Large Incidence," AIAA Paper No. 83-0034, 21st Aerospace Sciences Meeting, January 1983.

7. M. M. Rai and D. S. Chaussee, "New Implicit Boundary Procedures: Theory and Applications," AIAA Paper No. 83-0123, 21st Aerospace Sciences Meeting, January 1983.

8. M. M. Rai, D. S. Chaussee, and Y. M. Risk, "Calculation of Viscous Supersonic Flows Over Finned Bodies," AIAA Paper No. 83-1667, Danvers, MA, July 1983.

9. J. U. Jettmar, "Calculations of Viscous Supersonic Flow Over Finned Bodies Using a 'Thin-Fin' Approximation," AIAA Paper No. 84-2114, AIAA Atmospheric Flight Mechanics Conference, August 1984.

10. P. Weinacht, B. J. Guidos, L. D. Kayser, and W. B. Sturek, "PNS Computations for Spinning and Fin-Stabilized Projectiles at Supersonic Velocities," AIAA Paper No. 84-2118, AIAA Atmospheric Flight Mechanics Conference, August 1984. (BRL Memorandum Report to be published)

11. L. B. Schiff and J. L. Steger, "Numerical Simulation of Steady Supersonic Viscous Flow," AIAA Paper No. 79-0130, 17th Aerospace Sciences Meeting, January 1979.

12. R. Beam and R. F. Warming, "An Implicit Factored Scheme for the Compressible Navier-Stokes Equations," AIAA Journal, Vol. 16, No. 4, 1978, pp. 85-129.

REFERENCES (Cont'd)

13. R. P. Reklis and W. B. Sturek, "Surface Pressure Measurements on Slender Bodies at Angle of Attack at Supersonic Speeds," U.S. Army Ballistic Research Laboratory, Aberdeen Proving Ground, Maryland, ARBRL-MR-02876, November 1978. (AD A064097)

14. C. J. Nietubicz and K. O. Opalka, "Supersonic Wind Tunnel Measurements of Static and Magnus Aerodynamic Coefficients for Projectile Shapes with Tangent and Secant Ogive Noses," U.S. Army Ballistic Research Laboratory, Aberdeen Proving Ground, Maryland, ARBRL-MR-02991, February 1980. (AD A083297)

15. L. D. Kayser and W. B. Sturek, "Turbulent Boundary Layer Measurements on the Boattail Section of a Yawed, Spinning Projectile Shape at Mach 3.0," U.S. Army Ballistic Research Laboratory, Aberdeen Proving Ground, Maryland, ARBRL-MR-02880, November 1978. (AD A065355)

16. F. Brandon, "private communications," unpublished wind tunnel data, U.S. Army Ballistic Research Laboratory, Aberdeen Proving Ground, Maryland.

17. D. S. Chaussee, J. L. Patterson, P. Kutler, T. Pulliam, and J. L. Steger, "A Numerical Simulation of Hypersonic Viscous Flow Over Arbitrary Geometries at High Angle of Attack," AIAA Paper No. 81-0050, January 1981.

18. A. B. Wardlaw, Jr., F. P. Baltakis, J. M. Solomon, and L. B. Hackerman, "An Inviscid Computational Method for Tactical Missile Configurations," NSWC TR 81-457.

19. Unpublished range data, U.S. Army Ballistic Research Laboratory, Aberdeen Proving Ground, Maryland.

LIST OF SYMBOLS

a = speed of sound

C_m = pitching moment coefficient

C_{m_α} = $dC_m/d\alpha$, slope of the pitching moment coefficient

C_N = normal force coefficient

C_{N_α} = $dC_N/d\alpha$, slope of the normal force coefficient

C_Y = Magnus (side) force coefficient

D = diameter of model

e = total energy per unit volume of fluid, normalized by $\rho_\infty a_\infty^2$

$\hat{E}_s, \hat{F}, \hat{G}$ = flux vectors of transformed gas dynamic equation

L = projectile length

M = Mach number

P = pressure normalized by $\rho_\infty a_\infty^2$

PD/V = nondimensional spin rate about model axis

Re = Reynold's number per unit length, $\rho_\infty M_\infty a_\infty/\mu_\infty$

$\hat{Re}$ = Reynold's number, $\rho_\infty a_\infty D/\mu_\infty$

R_{e_D} = Reynold's number based on diameter $\rho_\infty M_\infty a_\infty D/u_\infty$

$\hat{S}$ = viscous flux vector

u, v, w = Cartesian velocity components along the x, y, z axis, respectively, normalized by a_∞

x, y, z = physical Cartesian coordinates

y^+ = distance from wall in law of the wall coordinates

α = angle of attack

μ = coefficient of viscosity, normalized by free stream value

μ_t = turbulent eddy viscosity coefficient

ξ, η, ζ = computational coordinates in the axial, circumferential, and radial directions

LIST OF SYMBOLS (Cont'd)

ρ = density, normalized by free-stream density

τ = shear stress

ϕ = circumferential angular coordinate

ω = local vorticity vector

Subscripts

∞ = free-stream conditions

w = body surface values

DISTRIBUTION LIST

No. of Copies	Organization
12	Administrator Defense Technical Info Center ATTN: DTIC-DDA Cameron Station Alexandria, VA 22304-6145
1	HQDA DAMA-ART-M Washington, DC 20310
1	Commander US Army Materiel Command ATTN: AMCDRA-ST 5001 Eisenhower Avenue Alexandria, VA 22333-0001
6	Commander Armament R&D Center US Army AMCCOM ATTN: SMCAR-TDC SMCAR-TSS SMCAR-LCA-F Mr. D. Mertz Mr. A. Loeb Mr. H. Hudgins Mr. E. Friedman Dover, NJ 07801
1	Commander US Army Armament, Munitions and Chemical Command ATTN: SMCAR-ESP-L Rock Island, IL 61299
1	Director Benet Weapons Laboratory Armament R&D Center US Army AMCCOM ATTN: SMCAR-LCB-TL Watervliet, NY 12189
1	Commander US Army Aviation Research and Development Command ATTN: AMSAV-E 4300 Goodfellow Blvd St. Louis, MO 63120
1	Director US Army Air Mobility Research and Development Command Ames Research Center Moffett Field, CA 94035
1	Commander US Army Communications - Electronics Command ATTN: AMSEL-ED Fort Monmouth, NJ 07703
1	Commander ERADCOM Technical Library ATTN: DELSD-L (Reports Section) Fort Monmouth, NJ 07703-5301
3	Commander US Army Missile Command Research, Development & Engineering Center ATTN: AMSMI-RD Dr. Bill Walker Mr. R. Deep Redstone Arsenal, AL 35898
1	Director US Army Missile & Space Intelligence Center ATTN: AIAMS-YDL Redstone Arsenal, AL 35898
1	Commander US Army Tank Automotive Command ATTN: AMSTA-TSL Warren, MI 48397-5000
1	Director US Army TRADOC Systems Analysis Activity ATTN: ATAA-SL White Sands Missile Range, NM 88002
1	Commander US Army Research Office P. O. Box 12211 Research Triangle Park, NC 27709

DISTRIBUTION LIST

No. of Copies Organization

1 Commander
US Naval Air Systems Command
ATTN: AIR-604
Washington, D. C. 20360

2 Commander
US Naval Surface Weapons Center
ATTN: Dr. T. Clare, Code DK20
Dr. F. Moore
Dahlgren, VA 22448-5000

2 Commander
US Naval Surface Weapons Center
ATTN: Dr. U. Jettmar
Silver Spring, MD 20902-5000

1 Commander
US Naval Weapons Center
ATTN: Code 3431, Tech Lib
China Lake, CA 93555

1 Commander
US Army Development and
Employment Agency
ATTN: MODE-TED-SAB
Fort Lewis, WA 98433

1 Director
NASA Langley Research Center
ATTN: MS-185, Tech Lib
Langley Station
Hampton, VA 23365

2 Commandant
US Army Infantry School
ATTN: ATSH-CD-CSO-OR
Fort Benning, GA 31905

1 AFWL/SUL
Kirtland AFB, NM 87117

1 Air Force Armament Laboratory
ATTN: AFATL/DLODL
Eglin AFB, FL 32542-5000

No. of Copies Organization

3 Director
NASA Ames Research Center
ATTN: MS-202A-14,
Dr. P. Kutler
MS-202-1, Dr. T. Pulliam
Prof. J. Steger
MS-227-8, Dr. L. Schiff
Moffett Field, CA 94035

3 Sandia Laboratories
ATTN: Division No. 1331
Mr. H. R. Vaughn
Dr. F. Blottner
Mr. G. R. Eisler
P.O. Box 580
Albuquerque, NJ 87184

1 AEDC
Calspan Field Services
ATTN: MS 600 (Dr. John Benek)
AAFS, TN 37389

1 Bendix Guided Systems Division
ATTN: MS 2/17A, S. Wasserman
Teterboro, NJ 07608

1 University of California, Davis
Department of Mechanical
Engineering
ATTN: Prof. H.A. Dwyer
Davis, CA 95616

1 Virginia Polytechnic Institute
& State University
ATTN: Dr. Clark H. Lewis
Department of Aerospace & Ocean
Engineering
Blacksburg, VA 24061

1 University of Delaware
Mechanical and Aerospace
Engineering Department
ATTN: J.E. Danberg
Newark, DE 19711

DISTRIBUTION LIST

10 Central Intelligence Agency
Office of Central Reference
Dissemination Branch
Room GE-47 HQS
Washington, DC 20502

Aberdeen Proving Ground

Dir, USAMSAA
ATTN: AMXSY-D
AMXSY-MP, H. Cohen

Cdr, USATECOM
ATTN: AMSTE-TO-F

Cdr, CRDC, AMCCOM
SMCCR-RSP-A
SMCCR-MU
SMCCR-SPS-IL

USER EVALUATION SHEET/CHANGE OF ADDRESS

This Laboratory undertakes a continuing effort to improve the quality of the reports it publishes. Your comments/answers to the items/questions below will aid us in our efforts.

1. BRL Report Number________________________Date of Report__________

2. Date Report Received____

3. Does this report satisfy a need? (Comment on purpose, related project, or other area of interest for which the report will be used.)________________

____

____

4. How specifically, is the report being used? (Information source, design data, procedure, source of ideas, etc.)_______________________________

____

____

5. Has the information in this report led to any quantitative savings as far as man-hours or dollars saved, operating costs avoided or efficiencies achieved, etc? If so, please elaborate.____________________________________

____

____

6. General Comments. What do you think should be changed to improve future reports? (Indicate changes to organization, technical content, format, etc.)

____

____

____

CURRENT ADDRESS

____
Name
____
Organization
____
Address
____
City, State, Zip

7. If indicating a Change of Address or Address Correction, please provide the New or Correct Address in Block 6 above and the Old or Incorrect address below.

OLD ADDRESS

____
Name
____
Organization
____
Address
____
City, State, Zip

(Remove this sheet along the perforation, fold as indicated, staple or tape closed, and mail.)

END

DTIC

8-86